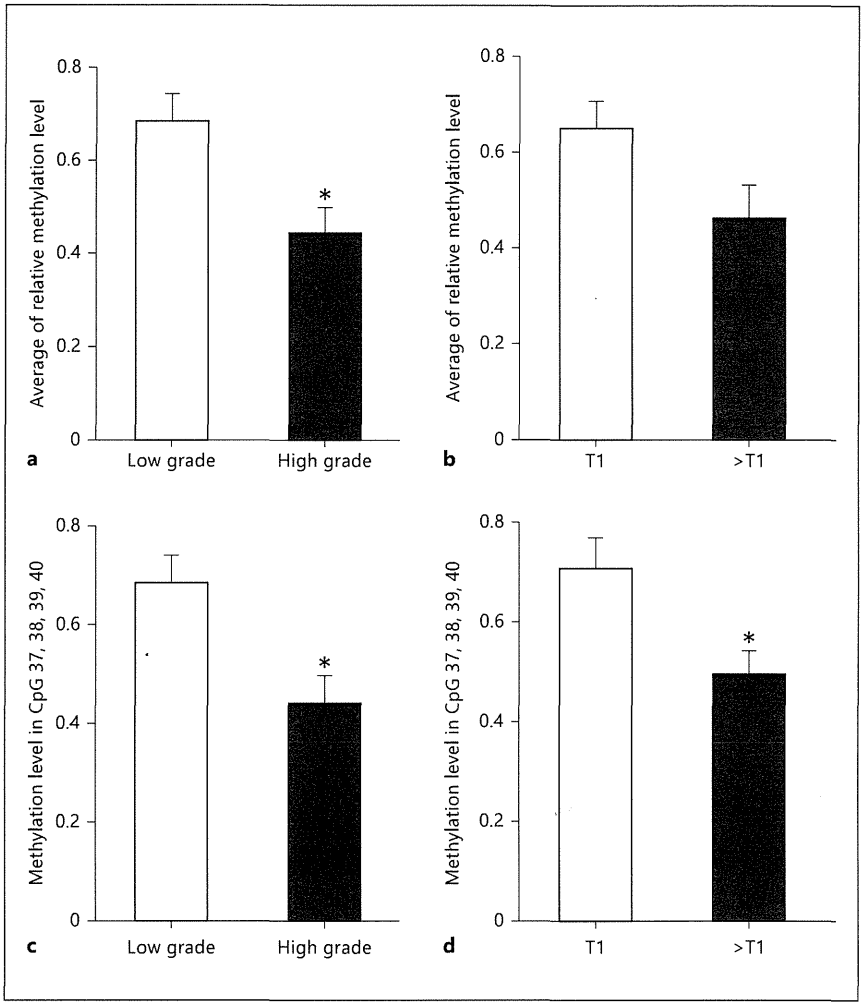

Fig. 2. Analysis of the association between methylation status of *ZAR1* exon 1/intron 1 CpGi and clinical characteristics. **a**, **b** The average methylation levels of *ZAR1* exon 1/intron 1 CpGi were compared among samples of different pathological grades (**a**) or T stages (**b**). **c**, **d** The average methylation levels of CpG 37, 38, 39, and 40 were compared among the samples of different pathological grades (**c**) or T stages (**d**). Statistical significance was examined using the Mann-Whitney test. * $p < 0.05$, bars = SD.

5′-cagtaatacgactcactatagggagaaggctACAAAACCAAACCCAAAAAAAACAC-3′. The tag sequence needed for transcription by T7-RNA polymerase is shown in lower-case. An initial denaturation step of 15 min at 94°C was followed by amplification for 45 cycles of 94°C for 20 s, 56°C for 30 s, and 72°C for 1 min, and then a final elongation step of 72°C for 3 min.

Subsequently, the PCR products were treated with shrimp alkaline phosphatase and subjected to in vitro transcription with T7 RNA polymerase. After RNase cleavage, the samples were desalted and spotted on a 384-pad SpectroCHIP (Sequenom) using a MassARRAY nanodispenser, followed by spectral acquisition using MassARRAY Analyzer Compact MALDI-TOF mass spectrometry (Sequenom). Resultant methylation calls were performed using the EpiTYPER software v. 1.0 (Sequenom) to generate quantitative results for each CpG site or an aggregate of multiple CpG sites.

A standard curve of quantitative DNA methylation analysis was drawn using 0, 50, and 100% methylated samples. The relative amount of methylation was calculated by comparing the difference in signal intensity between mass signals derived from methylated and nonmethylated DNA.

Statistical Analysis

To evaluate the association between clinicopathological findings and the methylation levels of *ZAR1* exon 1/intron 1 CpGi, the χ^2 test was used for pathological diagnosis and pathological N stage, and Fisher's exact test for cytology and pathological T stage. Mann-Whitney test was applied to assess differences in *ZAR1* methylation levels between the two groups of bladder cancer specimens of different stages or muscle invasion status. In both tests, $p < 0.05$ was considered statistically significant. Statistical analyses were performed using the SPSS statistical package.

Result

Clinical Characteristics of Bladder Cancer Cases

The samples from cases 1–13 were obtained by transurethral resection of the bladder tumor, whereas the

rest were by total cystectomy. The samples from cases 1–12 are non-muscle-invasive urothelium carcinomas (table 1). Of the 20 bladder cancers, 11 samples were low grade, whereas the rest were high grade.

Methylation Status of ZAR1

We examined the methylation levels of CpGi on *ZAR1* exon 1/intron 1, in which aberrant methylation levels were observed in mouse skin cancers in 20 human bladder cancer specimens. Representative data of the Sequenom MassARRAY analysis are presented as an epigram in figure 1a. Some of the tumor tissues showed low methylation levels in whole CpG sites on *ZAR1* exon 1/intron 1 CpGi. The high-grade cancers showed lower methylation levels in the *ZAR1* gene.

Figure 1b shows the average methylation levels of the entire region of *ZAR1* exon 1/intron 1 CpGi in the samples examined. Five out of 8 invasive cancers showed hypomethylation, in which the average methylation level was less than 50%; on the other hand, only 3 out of 12 samples were hypomethylated in the non-muscle-invasive group.

Low-Grade Methylation Status of ZAR1 Is Associated with Muscle-Invasive Characteristics

When the average methylation level of the whole *ZAR1* exon 1/intron 1 CpGi was compared among the samples of different grades, high-grade cancers showed significantly lower methylation levels than low-grade samples (fig. 2a). Tumors with higher muscle invasiveness (pathological T2 or more) showed lower methylation levels than T1 cancers (fig. 2b). Moreover, when each CpG site was individually analyzed, only the methylation levels of CpG 37, 38, 39, and 40 were significantly lower in both high-grade and muscle-invasive cancers than in low-grade and noninvasive tumors (table 2; fig. 2c, d).

Table 2. Relationship between methylation status of CpG 37, 38, 39, and 40 and clinicopathological findings in bladder cancer (n = 20)

	Methylation status		
	hypo (n = 6)	hyper (n = 14)	p value
Cytology			
II	1	2	0.49
IIIa	2	5	
IIIb	1	4	
IV	0	2	
V	2	1	
Pathological diagnosis			
Low grade	1	10	0.020
High grade	5	4	
Pathological T stage			
1	2	10	0.14
2b	3	2	
3a	0	1	
3b	0	1	
4	1	0	
Pathological N stage			
N0	3	2	0.20
N1	0	1	

Statistical significance was examined using the χ^2 test for pathological diagnosis and pathological N stage and using Fisher's exact test for cytology and pathological T stage.

Discussion

The clinical course of bladder cancer shows a broad spectrum of aggressiveness and risk. Low-grade superficial bladder cancers have minimal risk of progression to death, whereas high-grade muscle-invasive cancers are often lethal. Characterization of genomic methylation patterns is as a powerful tool for the prediction of disease outcome and sensitivity to treatment [10, 11]. The clinical importance of distinct genome methylation patterns as molecular markers has been shown in various malignancies, including bladder cancer [11, 12].

Classification of bladder cancer plays an important role in determining the appropriate treatment strategy and to predict outcomes. Transurethral resection is the gold standard method for defining the muscle invasiveness of bladder cancer. The most widely adopted noninvasive urine test is cytology, which has good specificity and sensitivity for the detection of high-grade tumors, but poor sensitivity for low-grade tumors [13] and often takes time to generate results [14]. To discover novel markers that are more specific and sensitive in detecting bladder cancer, we examined the methylation status of *ZAR1*, which has been reported to be aberrantly methylated in mouse skin tumors and human tumors such as melanoma, brain tumor, and hepatocellular carcinoma [6–8].

The present study is the first to demonstrate that hypomethylation of the *ZAR1* gene was implicated in a high proportion of muscle-invasive bladder cancers. In particular, the methylation levels of specific CpG sites such as CpG 37–40 have been strongly associated with tumor grade and muscle invasiveness. This result indicated that hypomethylation of the *ZAR1* region could serve as an epigenetic marker for advanced bladder cancer. Aberrant

methylation of DNA is a favorable candidate for a cancer biomarker because it can easily be detected using a well-known technique and a small amount of each sample. In addition, there is growing evidence that epigenetic alterations occur at the initial steps of tumorigenesis. Aberrant methylation could therefore serve as an effective marker for the early detection of cancer.

ZAR1 is an ovary-specific maternal factor that plays a key role in the initiation of embryogenesis; its involvement in tumor generation and/or development is unclear. Although we did not examine the expression level of the *ZAR1* transcript due to the lack of specimens to obtain a sufficient amount of quality RNA, the previous study examining malignant melanomas clarified that the methylation level of *ZAR1* exon 1/intron 1 CpGi was associated with an increased expression of the *ZAR1* transcript [6]. This report indicates that aberrant methylation of *ZAR1* exon 1/intron 1 CpGi could also result in the aberrant expression of this transcript in bladder cancer tissues. Further analysis is needed to elucidate the role of this gene in the development of bladder cancer.

The present study showed that hypomethylation of the *ZAR1* gene could serve as a biomarker for the detection of high-grade/muscle-invasive bladder cancer. Further optimization and large-scale clinical trials are needed to further validate our findings. There is also a need to develop a technique to detect aberrantly methylated DNA, including *ZAR1*, from urine or blood samples from patients.

Acknowledgments

This work was supported by a Nihon University Multidisciplinary Research Grant (2006–2007), the Academic Frontier Project for 2006 Project for Private Universities, a matching fund subsidy from MEXT (to Hiroki Nagase).

Disclosure Statement

None.

References

1 Enokida H, Nakagawa M: Epigenetics in bladder cancer. Int J Clin Oncol 2008;13:298–307.
2 Holmang S, Hedelin H, Anderstrom C, Johansson SL: The relationship among multiple recurrences, progression and prognosis of patients with stages Ta and T1 transitional cell cancer of the bladder followed for at least 20 years. J Urol 1995;153:1823–1826; discussion 1826–1827.
3 Sidransky D: Emerging molecular markers of cancer. Nat Rev Cancer 2002;2:210–219.
4 Holliday R, Pugh JE: DNA modification mechanisms and gene activity during development. Science 1975;187:226–232.
5 Moore LE, Pfeiffer RM, Poscablo C, Real FX, Kogevinas M, Silverman D, Garcia-Closas R, Chanock S, Tardon A, Serra C, Carrato A, Dosemeci M, Garcia-Closas M, Esteller M, Fraga M, Rothman N, Malats N: Genomic DNA hypomethylation as a biomarker for bladder cancer susceptibility in the Spanish Bladder Cancer Study: a case-control study. Lancet Oncol 2008;9:359–366.
6 Shinojima Y, Terui T, Hara H, Kimura M, Igarashi J, Wang X, Kawashima H, Kobayashi Y, Muroi S, Hayakawa S, Esumi M, Fujiwara K, Ghosh S, Yamamoto T, Held W, Nagase H: Identification and analysis of an early diagnostic marker for malignant melanoma: ZAR1 intra-genic differential methylation. J Dermatol Sci 2010;59:98–106.
7 Watanabe T, Yachi K, Ohta T, Fukushima T, Yoshino A, Katayama Y, Shinojima Y, Terui T, Nagase H: Aberrant hypermethylation of non-promoter zygote arrest 1 (ZAR1) in human brain tumors. Neurol Med Chir 2010;50:1062–1069.
8 Takagi K, Fujiwara K, Takayama T, Mamiya T, Soma M, Nagase H: DNA hypermethylation of zygote arrest 1 (ZAR1) in hepatitis C virus positive related hepatocellular carcinoma. Springerplus 2013;2:150.
9 Ehrich M, Nelson MR, Stanssens P, Zabeau M, Liloglou T, Xinarianos G, Cantor CR, Field JK, van den Boom D: Quantitative high-throughput analysis of DNA methylation patterns by base-specific cleavage and mass spectrometry. Proc Natl Acad Sci USA 2005;102:15785–15790.
10 Woo HD, Kim J: Global DNA hypomethylation in peripheral blood leukocytes as a biomarker for cancer risk: a meta-analysis. PloS One 2012;7:e34615.
11 Wolff EM, Chihara Y, Pan F, Weisenberger DJ, Siegmund KD, Sugano K, Kawashima K, Laird PW, Jones PA, Liang G: Unique DNA methylation patterns distinguish noninvasive and invasive urothelial cancers and establish an epigenetic field defect in premalignant tissue. Cancer Res 2010;70:8169–8178.
12 Han H, Wolff EM, Liang G: Epigenetic alterations in bladder cancer and their potential clinical implications. Adv Urol 2012;2012:546917.
13 Lotan Y, Roehrborn CG: Sensitivity and specificity of commonly available bladder tumor markers versus cytology: results of a comprehensive literature review and meta-analyses. Urology 2003;61:109–118; discussion 118.
14 Cheung G, Sahai A, Billia M, Dasgupta P, Khan MS: Recent advances in the diagnosis and treatment of bladder cancer. BMC Med 2013;11:13.

Cancer Science
Japanese Cancer Association JCA
Open Access

Pyrrole-imidazole polyamide targeted to break fusion sites in TMPRSS2 and ERG gene fusion represses prostate tumor growth

Daisuke Obinata,[1,2,9] Akiko Ito,[1,9] Kyoko Fujiwara,[3,9] Ken-Ichi Takayama,[2,4] Daisaku Ashikari,[1,2] Yasutaka Murata,[1] Kenya Yamaguchi,[1] Tomohiko Urano,[2,4] Tetsuya Fujimura,[5] Noboru Fukuda,[6] Masayoshi Soma,[3] Takayoshi Watanabe,[7] Hiroki Nagase,[7] Satoshi Inoue[2,4,8] and Satoru Takahashi[1]

[1]Department of Urology, Nihon University School of Medicine, Tokyo; [2]Department of Anti-Aging Medicine, Graduate School of Medicine, The University of Tokyo, Tokyo; [3]Division of General Medicine, Department of Medicine, Nihon University School of Medicine, Tokyo; [4]Department of Geriatric Medicine, The University of Tokyo, Tokyo; [5]Department of Urology, Graduate School of Medicine, The University of Tokyo, Tokyo; [6]Department of Advanced Medicine and Advanced Research Institute of Sciences and Humanities, Nihon University School of Medicine, Tokyo; [7]Chiba Cancer Center Research Institute, Chiba; [8]Division of Gene Regulation and Signal Transduction, Research Center for Genomic Medicine, Saitama Medical University, Saitama, Japan

Key words

Androgen receptor, fusion gene, prostate cancer, pyrrole–imidazole polyamide, *TMPRSS2-ERG*

Correspondence

Satoshi Inoue, Department of Anti-Aging Medicine, Graduate School of Medicine, University of Tokyo, 7-3-1, Hongo, Bunkyo-ku, Tokyo 113-8655, Japan.
Tel: 81-3-5800-8834; Fax: +81-3-5800-9126;
E-mail: INOUE-GER@h.u-tokyo.ac.jp

[9]These authors contribute equally to this work.

Funding information

This work was supported by Grants of the Cell Innovation Program (to S. I.) from the Ministry of Education, Culture, Sports, Science and Technology (MEXT), Japan; by the 2011–2015 Strategic Research Foundation for Private Universities (to M. S., D. O., K. F., N. F. and S. T.) from the MEXT-Supported Program; by Grants (to D. O., S. I., T. U. and S. T) from the Japan Society for the Promotion of Science, Japan; by the 2010 Research Grant of the 60th Anniversary Memorial Fund (to D. O.) from the Nihon University Medical Alumni Association; by the Young Researcher Promotion Grant (to D. O.) from The Japanese Urological Association; and by the Program for Promotion of Fundamental Studies in Health Sciences (S. I.), National Institute of Biomedical Innovation, Japan.

Received May 10, 2014; Revised July 18, 2014; Accepted July 23, 2014

Cancer Sci **105** (2014) 1272–1278

doi: 10.1111/cas.12493

Aberrant overexpression of ERG induced by the *TMPRSS2-ERG* gene fusion is likely involved in the development of prostate cancer. Synthetic pyrrole–imidazole (PI) polyamides recognize and attach to the minor groove of DNA with high affinity and specificity. In the present study, we designed a PI polyamide targeting *TMPRSS2-ERG* translocation breakpoints and assessed its effect on human prostate cancer cells. Our study identified that this PI polyamide repressed the cell and tumor growth of androgen-sensitive LNCaP prostate cancer cells. Targeting of these breakpoint sequences by PI polyamides could be a novel approach for the treatment of prostate cancer.

The androgen receptor (AR) plays a key role in the physiological development of the normal prostate epithelium as well as in the onset and progression of prostate cancer.[1] AR is a member of the nuclear receptor superfamily and functions as a ligand-dependent transcription factor.[2] Upon activation by androgens, AR translocates into the nucleus and binds to androgen responsive elements (ARE).

Recently, fusion of the prostate-specific androgen-regulated TMPRSS2 gene to the E26 transformation-specific (ETS) family transcription factor gene *ERG* was reported as a common event in prostate cancer.[3–7] ETS family members modulate many cellular functions, including proliferation, apoptosis, differentiation, tissue remodeling, migration, invasion and angiogenesis.[8] Altered expression or properties of ETS transcription regulators affect the control of these processes and are involved in carcinogenesis and cancer progression. Several studies have demonstrated that ETS family gene re-arrangements are linked to clinicopathological indicators in prostate cancer.[6,9,10] Because TMPRSS2, 5′-fusion partners, are upregulated by androgen, AR has been supposed to be important to

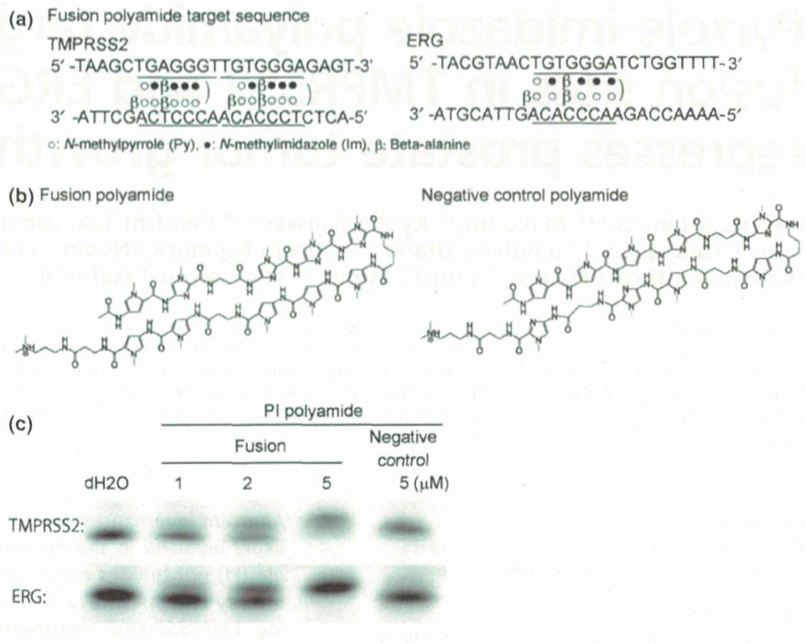

Fig. 1. Target sequence and structure of synthetic pyrrole–imidazole (PI) polyamide that targets the break fusion sites in TMPRSS2 and ERG. (a) PI polyamide targeting break fusion sites. The polyamide was designed to bind to the break fusion site in TMPRSS2 and ERG. (b) Structure of the fusion polyamide and negative control polyamide. They were synthesized by employing a solid-phase method and purified by high performance liquid chromatography (0.1% AcOH/CH3CN, 0–66% linear gradient, 0–20 min, 254 nm, through a Chemcobond 5-ODS-H column). (c) Gel mobility shift assay and distribution of fluorescein isothiocyanate (FITC)-labeled PI polyamide *in vitro*. FITC-labeled DNA corresponding to the break fusion sites in TMPRSS2 was synthesized and incubated with vehicle (water), fusion PI polyamide, or negative control PI polyamide for 1 h at 37°C and loaded onto a 20% polyacrylamide gel.

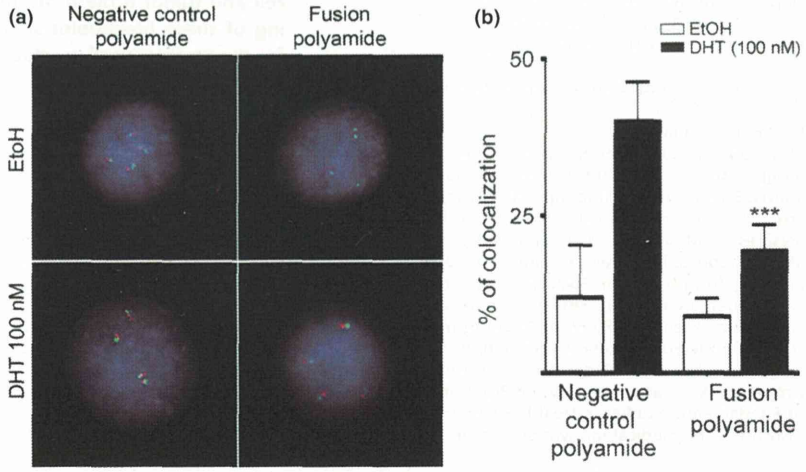

Fig. 2. Presence of the fusion polyamide resulted in decreased androgen receptor-induced and chromosomal interactions of TMPRSS2 and ERG loci. (a, b) Following treatment of LNCaP cells with the fusion polyamide for 72 h, cells were stimulated with dihydrotestosterone (DHT) for 24 h, and FISH was performed with TMPRSS2 (green) and ERG (red) probes. (***$P < 0.0001$ versus negative control polyamide).

regulate the fusion of genes in prostate cancer. A recent study shows that AR induces intronic binding sites in TMPRSS2 and ERG to facilitate specific chromosomal translocations by utilizing a common motif (TGT/AGGGA/T: break fusion site) for break/ligation in the human prostate cancer cell line LNCaP, which does not harbor *TMPRSS2-ERG* endogenously.[11–14]

Pyrrole–imidazole (PI) polyamides are small synthetic molecules that recognize and form non-covalent bonds to the minor groove of DNA, followed by inhibition of DNA–protein interactions with high affinity and sequence specificity.[15–17] DNA recognition depends on a code of side-by-side pairing of pyrrole and imidazole in the hairpin polyamide, which binds to the minor groove. A pairing of imidazole opposite pyrrole targets for the G–C base pair, and pyrrole–pyrrole targets for both T–A and A–T base pairs. Recently, various types of sequence-specific PI polyamides have been developed to control gene expression.[18–22] These investigations indicate that targeted PI polyamides could be potential gene silencers for the treatment of cancer. The aim of the present study is to investigate the effects of a PI polyamide targeting the *TMPRSS2-ERG* translocation break fusion site (fusion polyamide) in prostate cancer. We demonstrate that the fusion polyamide decreases the expression of *TMPRSS2-ERG* and ERG in LNCaP cells. In addition, we show that this polyamide represses the growth and migration of prostate cancer cells *in vitro* and *in vivo*.

Material and Methods

Cell culture, treatment with pyrrole–imidazole polyamide and antibody. The human prostate cancer cell lines LNCaP, VCaP and PC3 were purchased from the American Type Culture Collection (Rockville, MD, USA). LNCaP cells were maintained as previously described;[23] VCaP and PC3 cells were cultured in DMEM supplemented with 10% FBS. PI polyamides were synthesized at Nihon University (Tokyo, Japan), as previously described.[18] LNCaP cells were treated with negative control PI polyamide (negative control) and PI polyamide that targets break fusion sites (fusion polyamide) as previously described.[18] A rabbit polyclonal anti-cleaved caspase-3

antibody was purchased from Cell Signaling Technology (Danvers, MA, USA).

DNA binding assay. FITC-labeled oligonucleotides were synthesized for gel mobility shift assays as described below.

TMPRSS2: 5′-FITC-TGTTAAGCTGAGGGTTGTGGGAGA GTGTTTTTCACTCTCCCACAACCCTCAGCTTAACA-3′.
ERG: 5′-FITC-TTCATGTTTGTGGGTGGGTGTATGTTTT TCATACACCCACCCACAAACATGAA-3′.

Both TMPRSS2 and ERG nucleotides contain the sequence TGT/AGGGA/T, which is the break fusion site in TMPRSS2 and ERG. Next, 1 μM of FITC-labeled oligonucleotides were dissolved in annealing buffer (20 mM Tris–HCl, 2 mM EDTA, 200 mM NaCl) and incubated at 100°C for 3 min. The solution was cooled down gradually to 30°C in the next 70 min to anneal the oligonucleotides in such a way that hairpin structures were formed. Then, 15 μL of annealed oligonucleotides and 5 μL of 2, 4 or 20 μM polyamides were mixed and incubated at 37°C for 1 h. The mixtures were separated by electrophoresis in 1× Tris-buffered EDTA on a 4–20% acrylamide gel and visualized with the luminescent image analyzer LAS-4000 (Fujifilm, Tokyo, Japan).

FISH. LNCaP cells were stimulated with vehicle or 100 nM dihydrotestosterone (DHT) in the presence of negative control or fusion polyamide for 24 h. Isolation of nuclear proteins and DNA-FISH were carried out according to methods previously described (Ourgenic, Tokushima, Japan).[24] The probes were synthesized by Integrated DNA Technologies (Coralville, IA, USA) as listed bellow:

ERG
Biotin-GACTCCAGGAGCGCTCCCCAGAATCCCCTTCC TTAACCCAAACTCGAGCC.
TMPRSS2
FITC(FAM)-GATCTTTGGAGACCCGAGGAAAGCCGTG TTGACCAAAAGCAAGACAAATG.

Quantitative RT-PCR. Total RNA extraction, first-strand cDNA synthesis and quantitative RT-PCR (qRT-PCR) were performed as previously described.[23] LNCaP cells were treated with 5 μM of negative control PI polyamide or 1 or 5 μM

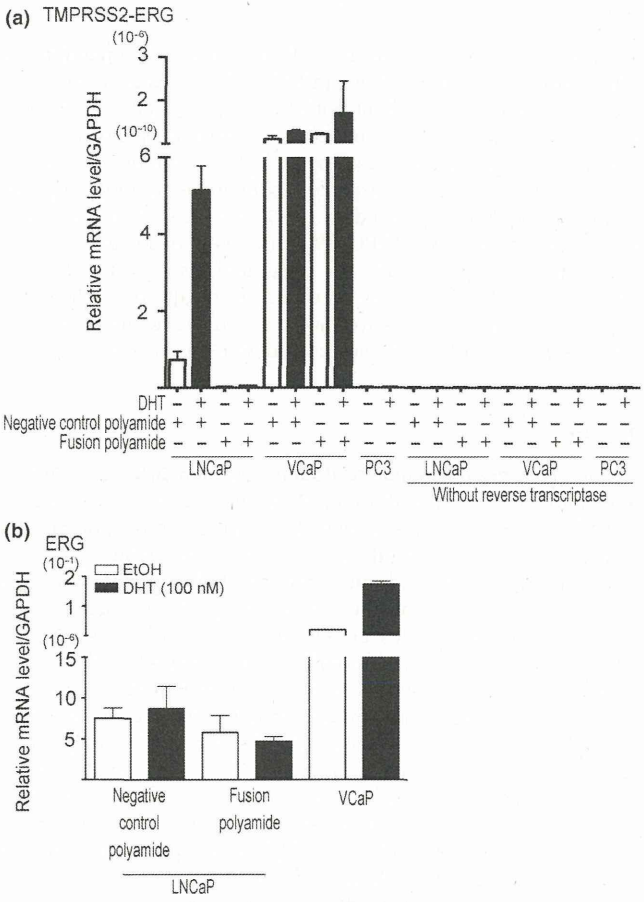

Fig. 3. Efficacy of the pyrrole–imidazole (PI) polyamide targeting the break fusion site for fusion transcript and endogenous ERG expressions. (a, b) The presence of the fusion polyamide resulted in reduced expression of *TMPRSS2-ERG* and ERG expressions. LNCaP cells were treated with 5 μM of negative control PI polyamide or 5 μM of fusion polyamide (Fusion). Two days after treatment with DHT (100 nM), the mRNA expression levels of *TMPRSS2-ERG* and ERG were analyzed by quantitative RT-PCR. We used VCaP cells as positive and PC3 cells as a negative control for *TMPRSS2-ERG* expression.

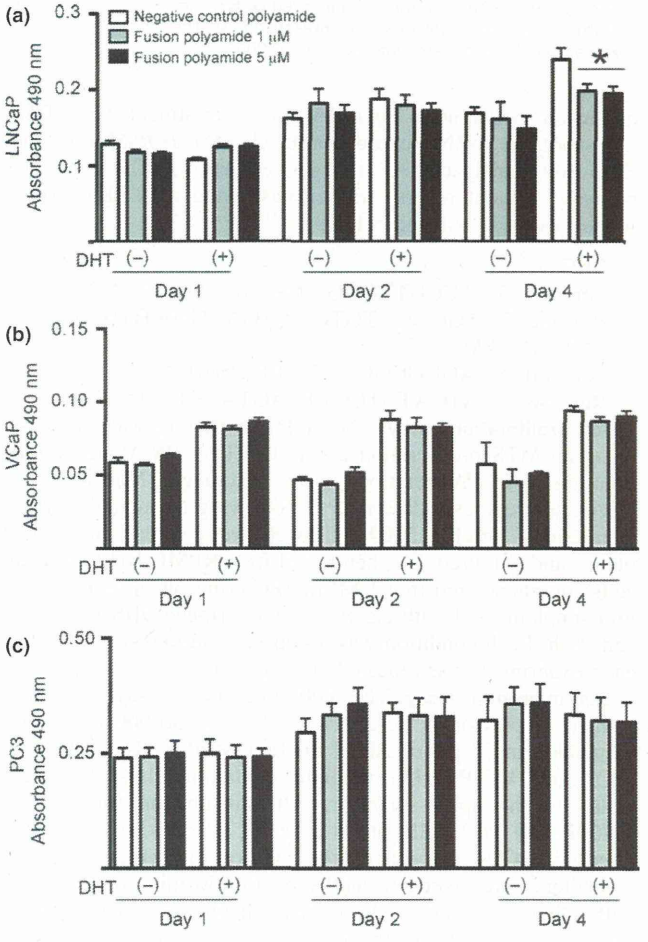

Fig. 4. Effect of the fusion polyamide on cell growth. The fusion polyamide reduced (a) LNCaP cell growth in an androgen-dependent manner. (b) VCaP cells and (c) PC3 cells in phenol red-free DMEM and LNCaP cells in phenol red-free RPMI medium were treated for 48 h with 5 μM of negative control polyamide (negative control) or 1 or 5 μM of pyrrole–imidazole (PI) polyamide targeting the break fusion site (fusion polyamide). After stimulation with 100 nM dihydrotestosterone (DHT), an MTS assay was performed to assess the cell proliferation rate of PI polyamide-treated cells. Results are presented as mean and SD of triplicate assays (*$P < 0.05$).

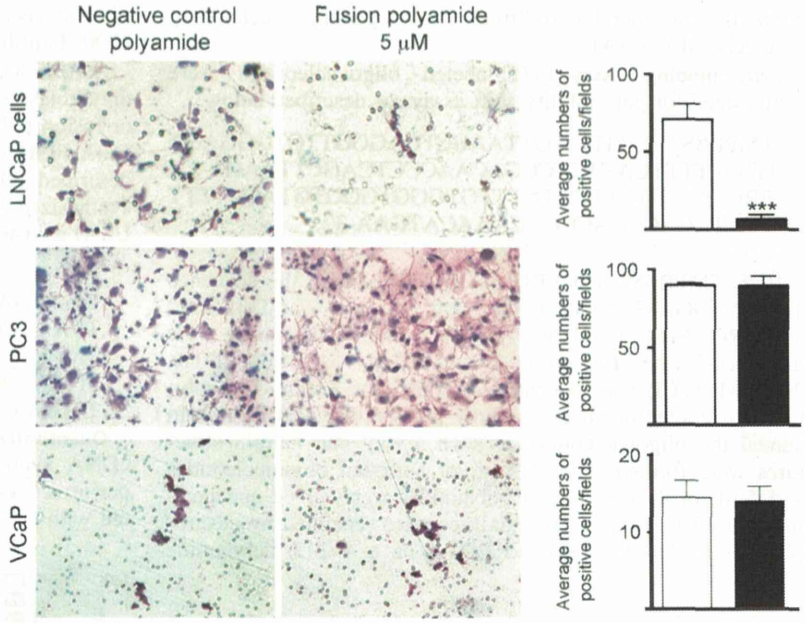

Fig. 5. Effect of the fusion polyamide on cell migration. Effect of the fusion polyamide on cell migration. A cell migration assay was performed to analyze the motility of fusion polyamide-treated LNCaP, PC3 and VCaP cells and negative control polyamide-treated cells. Migrated cells were stained with Giemsa solution. Right panel shows average number of cells that migrated through the PET filter. Five representative fields in each well were quantified to determine the number of migrated cells under a light microscope. Results are presented as the mean and SD of triplicate assays (***$P < 0.0001$).

of fusion polyamide. Two days after treatment with DHT (100 nM), the mRNA expression levels of *TMPRSS2-ERG* and ERG were analyzed. As a negative control, cDNA samples prepared without reverse transcriptase were used. The primer sequences were as listed below:[11,25]

ERG
Forward: 5′- ACCGTTGGGATGAACTACGGCA-3′
Reverse: 5′- TGGAGATGTGAGAGAAGGATGTCG
TMPRSS2-ERG
Forward: 5′- AGCGCGGCAGGTTATTCCA-3′
Reverse: 5′- ATCATGTCCTTCAGTAAGCCA-3′.

Cell proliferation assay. The cell growth rate was measured using an MTS proliferation assay (CellTiter 96 AQueous One Solution Cell Proliferation Assay; Promega, Madison, WI, USA), as previously described[26] following the manufacturer's instructions. Briefly, 5000 cells/well were seeded in 96-well plates and cultured in phenol red-free RPMI 1640 (LNCaP cells) or phenol red-free DMEM (PC3 and VCaP cells) medium supplemented with 2.5% charcoal-stripped FBS for 24, 48 and 96 h. Each condition was tested in quadruplicate wells and each experiment was repeated at least twice.

Cell migration assay. The cell migration assay was performed as previously described.[26] Briefly, 50 000 cells were suspended in 30 μL of RPMI 1640 (LNCaP cells) or DMEM (PC3 and VCaP cells) medium containing 10% FBS and added to the upper chamber. After incubation for 24 h in LNCaP and PC3 cells or 48 h in VCaP cells at 37°C in a humid 5% CO_2 atmosphere, the cells on the lower surface of the filter were fixed in methanol for 30 min, then stained with Giemsa solution (Muto Pure Chemicals, Tokyo, Japan) for 30 s. The cells on the lower surface were counted in at least five fields at a magnification of ×200 under a microscope.

Analysis of the *in vivo* effects of polyamides. Three million LNCaP cells were injected subcutaneously into each side of 7-week-old male nude mice ($n = 12$). When the tumor size reached 100 mm^3, fusion polyamide or negative control polyamide (6 mg/kg body weight) dissolved in dH_2O were injected via the tail vein once a week for 4 weeks. The tumor size was measured every week until 1 week after the final injection, at which point the animals were killed and dissected. Tumor tissues were collected and kept both frozen and fixed in 10% formalin for analysis. Immunohistochemistry analysis was performed as previously described.[25] The sections were incubated with the cleaved caspase-3 polyclonal antibody (1:100 dilution) overnight, followed by a 60-min incubation with Histofine Simple Stain MAX-PO (Nichirei, Tokyo, Japan).

Statistical analysis. Data are presented as mean ± SD or SEM. Statistical differences between the results of each group and its corresponding control were evaluated using Student's *t*-test. A *P*-value of <0.05 was considered significant.

Results

Binding of the polyamide to double-stranded DNA. The fusion polyamide was designed to bind to the break fusion site in TMPRSS2 and ERG. As a control, negative control polyamide, which does not bind to these sites, was used (Fig. 1a,b). To determine the binding affinity and specificity of polyamide to target DNA, gel mobility shift assays were performed. Whereas oligonucleotides containing the break fusion site of TMPRSS or ERG showed mobility retardation when they were incubated with the fusion polyamide, nucleotides incubated with negative control polyamide did not show a clear mobility shift. The degree of mobility shift by the fusion polyamide was shown to be dose-dependent (Fig. 1c). The distribution of FITC-labeled fusion polyamide and negative control polyamide in LNCaP cells are shown in Fig. S1. After 2 h of incubation of LNCaP cells with 5 μM of FITC-labeled polyamide, strong fluorescent signals were detected in nuclei.

Pyrrole–imidazole polyamide targeting the break fusion site decreased fusion transcript and endogenous ERG. Because previous reports show that *TMPRSS2-ERG* transcripts are induced in LNCaP cells by stimulation of DHT (100 nM) for 24 h,[11–14] we analyzed LNCaP cells treated with the same protocol. To determine whether the fusion polyamide affects DHT-dependent inter-chromosomal movement and *TMPRSS2-ERG* expression in LNCaP cells, we performed FISH analysis and

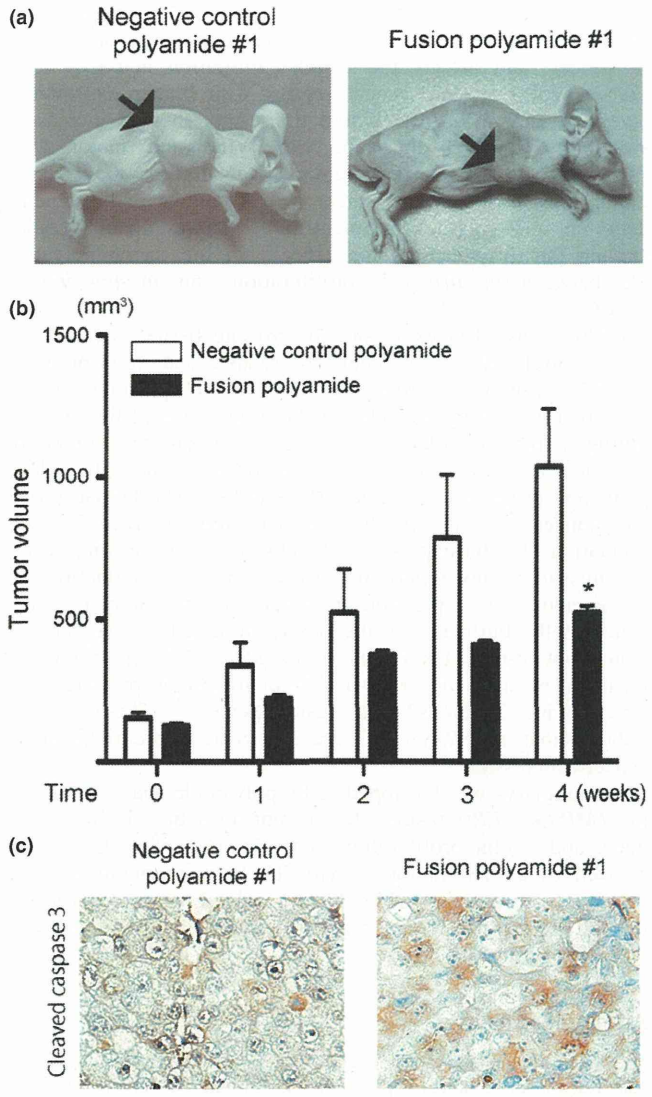

Fig. 6. The fusion polyamide represses tumor formation of LNCaP cells in nude mice. (a, b) Seven-week-old male mice were implanted with 3×10^6 tumor cells and fusion polyamide or negative control polyamide was injected into the tail vein once weekly. (a) Photographs of mice bearing tumors after 4 weeks of treatment with pyrrole–imidazole (PI) polyamide. (b) Treatment with the fusion polyamide significantly reduced the tumor volume compared to treatment with the negative control polyamide. Line plots, means of tumor volume (V mm^3) formed in mice; bars, SEM ($n = 6$ each), as determined by the formula: $V = 0.5 \times$ maximal diameter $\times$ middle diameter $\times$ minimal diameter. $^*P < 0.05$ for fusion polyamide versus negative control polyamide. (c) Representative image of immunohistochemistry for cleaved caspase-3 in tumor xenograft tissues. (Magnification: $\times$400.)

measured *TMPRSS2-ERG* expression levels using qRT-PCR. After DHT treatment, the number of cells showing co-localization of TMPRSS2 and ERG was significantly increased in LNCaP cells cultured in the presence of 5 μM of negative control polyamide (Fig. 2). This DHT-induced inter-chromosomal movement, however, was significantly decreased in cells cultured with 5 μM of fusion polyamide. Although the *TMPRSS2-ERG* transcript was significantly and constantly expressed in VCaP cells, which harbor this fusion gene, its expression was induced to a detectable level by the stimulation with DHT in LNCaP cells. The expression of the *TMPRSS2-ERG* transcript was significantly suppressed in the presence of 5 μM of the fusion polyamide compared with 5 μM of negative control polyamide in LNCaP cells. In contrast, the fusion polyamide did not affect its expression in VCaP cells (Fig. 3a). Moreover, we tested whether the fusion polyamide could downregulate endogenous *ERG* gene expression. Both 1 and 5 μM of fusion polyamide substantially reduced mRNA expression levels of ERG in LNCaP cells (Fig. 3b).

Fusion polyamide repressed cell growth and cell migration. To assess the effect of the fusion polyamide on the viability of prostate cancer cells, we analyzed the cell proliferation activity by MTS assay.[26] LNCaP cells treated with 1 and 5 μM fusion polyamide showed a significant decrease in cell proliferation after 96 h of DHT treatment compared to cells treated with negative control polyamide ($P < 0.05$; Fig. 4). The MTS assay also revealed that the fusion polyamide had no significant effect on cell proliferation in AR-negative and *TMPRSS2-ERG*-negative prostate cancer cell line PC3 cells and VCaP cells (Fig. 4). Next, we assessed the effects of the fusion polyamide on the migratory ability of LNCaP cells by conducting cell migration assays. Cell migration was significantly reduced in fusion polyamide-treated cells compared to negative control polyamide-treated cells ($P < 0.0001$, Fig. 5). Neither PC3 nor VCaP cells showed significant differences in average number of migratory cells between fusion polyamide-treated cells and negative control polyamide-treated cells (Fig. 5).

Fusion polyamide repressed tumor growth *in vivo*. Athymic male mice bearing LNCaP cell-derived tumors were treated with the fusion polyamide or negative control polyamide. Tumor growth was prominent in mice treated with the negative control polyamide, but it was substantially reduced in mice treated with the fusion polyamide (Fig. 6a,b). Moreover, the expression of cleaved caspase-3 tended to increase in LNCaP xenografts derived from mice treated with the fusion polyamide (Fig. 6c).

Discussion

Activation of AR signaling mediated by androgens promotes cancer progression. Several studies have shown that AR expression is positively correlated with standard clinical and pathologic parameters, including the Gleason grade, clinical stage, lymph node status, extracapsular extension and seminal vesicle invasion.[27,28] The reports of the fusion of TMPRSS2 with ETS family members in prostate cancer have opened a new field in prostate cancer research.[3,5–7,29–31] Approximately 80% of prostate tumors harbor genomic fusions of TMPRSS2 and members of the ETS family of transcription factors. Among them, approximately 50% contain *TMPRSS2-ERG* fusions.[32,33] Recently, urine testing to detect *TMPRSS2-ERG* has been reported to demonstrate significant correlation of the expression level of this fusion transcript with Gleason score, clinical stage and extracapsular extension of the tumor.[34,35] In addition, the expression of *TMPRSS2-ERG* promoted by AR has been associated with a poor clinical outcome.[36,37] Those findings indicate that evaluation of the expression level of *TMPRSS2-ERG* is valuable not only for diagnosis but also for predicting prognosis. Furthermore, it is also indicated that repressing the mechanism of *TMPRSS2-ERG* expression is crucial for the development of therapeutic approaches. In the present study, we attempted to develop a new compound that can repress the fusion gene formation and/or expression and to assess its effect on prostate cancer growth.

A previous report showed that the expression of fusion transcripts was inhibited by siRNA, which target specific components involved in homologous recombination of DNA.[11] Shao *et al.* (2012) report that siRNA targeting most common isoforms of the *TMPRSS2-ERG* fusion transcript efficiently suppressed the growth of prostate cancer *in vivo*.[38] Those data strongly suggest that inhibition of *TMPRSS2-ERG* fusion gene formation or expression could be a good therapeutic approach for prostate cancer. siRNA can effectively repress the expression of specific genes. However, there is a disadvantage in its application; that is, siRNA can be easily degraded by nucleases. One of the most important advantages of PI polyamide is that it is resistant to biological degradation (e.g. by nucleases and proteases). It can be taken up by cells and transported to nuclei without requiring any specific drug delivery system. Moreover, PI polyamide can inhibit DNA–protein interaction by binding to the minor groove of double-helical DNA with high affinity and sequence specificity.[15,16] Another important advantage is that intravenous, subcutaneous or peritoneal injections of PI polyamide have never induced significant health injuries when tested in mice and rats.[18,19,39,40] Raskatov *et al.*[41] report that intra-peritoneal or subcutaneous administration of 120 nmol/mouse (4.5–7 mg/kg body weight) of PI polyamide in cyclic form had an acute toxic effect on mice; however, they showed that the hairpin form of PI polyamide did not have any toxic effect at the same dose. In addition, Yang *et al.*[39] report that subcutaneous injection of PI polyamides targeting RNA polymerase II resulted in growth reduction in LNCaP xenografts without detectable DNA damage. Therefore, in the present study, we designed and examined PI polyamide, which binds to break fusion sites, to inhibit double-stranded breaks. It has been reported previously that PI polyamide that recognizes ARE suppresses DHT-dependent gene expression in LNCaP cells,[42] and it was revealed that this polyamide inhibits the binding of RNA polymerase II to the transcription start site of AR-driving genes.[39]

Our present data clearly show that this fusion polyamide suppresses the formation and expression of *TMPRSS2-ERG* fusion genes. In addition, it suppressed endogenous ERG expression and cellular proliferation in *in vitro* models and also induced cellular apoptosis in *in vivo* models. Interestingly, the effect of PI polyamide on the inhibition of cell migration and *in vivo* tumor growth appeared to be drastic compared to its inhibitory effect on *in vitro* cell proliferation. Recent study has shown that the *TMPRSS2-ERG* fusion gene expressed in prostate cancer changes tumor microenvironment to that associated with more aggressive phenotype of cancer, and affects the cellular migration activity.[43–45] For example, prostate cancer tissues with higher expression levels of *TMPRSS2-ERG* fusion transcripts showed increased vascular density, hyaluronan, von Willebrand factor and PDGFRβ, and decreased Caveolin-1. In addition, the *in vivo* tumor growth of prostate cancer cells is shown to be dependent on the microenvironment.[46,47] These factors could explain the difference of the efficacy of the fusion polyamide between *in vitro* cell proliferation and *in vivo* tumor growth.

Endogenous ERG expression in prostate tissues was shown to be correlated with biochemical relapse and poor prognosis.[48,49] Moreover, ERG overexpression in prostate cancer specimen is a strong predictor of the progression of the disease during active surveillance.[50] Recently, it has been reported that the *TMPRSS2–ERG* fusion gene product binds to the ERG locus and promotes wild-type ERG expression in human prostate cancers.[51] This mechanism activated the feed-forward regulation of ERG expression, thereby promoting prostate cancer invasion. This report also showed that the reduction of endogenous ERG expression prevented the invasion of prostate cancer cells. Furthermore, the report showed that overexpression of wild-type ERG was observed in 38% of clinically localized prostate cancers and 27% of metastatic prostate cancers bearing *TMPRSS2-ERG* fusion genes.[51] These reports indicate that *TMPRSS2-ERG* plays a critical role in prostate cancer progression.

In summary, we developed a PI polyamide that can target the *TMPRSS2-ERG* fusion site, prevent formation of the fusion gene, and inhibit proliferation and migration of LNCaP cells as well as *in vivo* tumor growth. The present findings show that break fusion sites, which have a critical role in the formation of AR-dependent fusion genes, could be a novel therapeutic target for prostate cancer.

Acknowledgments

The authors thank Ms Asako Oguni, Ms Noriko Sasaki and Mr Motoaki Kataba for technical support and Ms Emiko Hododa for secretarial assistance.

Disclosure Statement

The authors have no conflict of interest to declare.

References

1 Heinlein CA, Chang C. Androgen receptor in prostate cancer. *Endocr Rev* 2004; **25**: 276–308.
2 Mangelsdorf DJ, Thummel C, Beato M *et al.* The nuclear receptor superfamily: the second decade. *Cell* 1995; **83**: 835–9.
3 Tomlins SA, Rhodes DR, Perner S *et al.* Recurrent fusion of TMPRSS2 and ETS transcription factor genes in prostate cancer. *Science* 2005; **310**: 644–8.
4 Tomlins SA, Mehra R, Rhodes DR *et al.* TMPRSS2:ETV4 gene fusions define a third molecular subtype of prostate cancer. *Cancer Res* 2006; **66**: 3396–400.
5 Tomlins SA, Laxman B, Varambally S *et al.* Role of the TMPRSS2-ERG gene fusion in prostate cancer. *Neoplasia* 2008; **10**: 177–88.
6 Mehra R, Tomlins SA, Shen R *et al.* Comprehensive assessment of TMPRSS2 and ETS family gene aberrations in clinically localized prostate cancer. *Mod Pathol* 2007; **20**: 538–44.
7 Mehra R, Tomlins SA, Yu J *et al.* Characterization of TMPRSS2-ETS gene aberrations in androgen-independent metastatic prostate cancer. *Cancer Res* 2008; **68**: 3584–90.
8 Oikawa T, Yamada T. Molecular biology of the Ets family of transcription factors. *Gene* 2003; **303**: 11–34.
9 Wang J, Cai Y, Ren C, Ittmann M. Expression of variant TMPRSS2/ERG fusion messenger RNAs is associated with aggressive prostate cancer. *Cancer Res* 2006; **66**: 8347–51.
10 Perner S, Demichelis F, Beroukhim R *et al.* TMPRSS2:ERG fusion-associated deletions provide insight into the heterogeneity of prostate cancer. *Cancer Res* 2006; **66**: 8337–41.
11 Lin C, Yang L, Tanasa B *et al.* Nuclear receptor-induced chromosomal proximity and DNA breaks underlie specific translocations in cancer. *Cell* 2009; **139**: 1069–83.
12 Bastus NC, Boyd LK, Mao X *et al.* Androgen-induced TMPRSS2:ERG fusion in nonmalignant prostate epithelial cells. *Cancer Res* 2010; **70**: 9544–8.
13 Haffner MC, Aryee MJ, Toubaji A *et al.* Androgen-induced TOP2B-mediated double-strand breaks and prostate cancer gene rearrangements. *Nat Genet* 2010; **42**: 668–75.
14 Mani RS, Tomlins SA, Callahan K *et al.* Induced chromosomal proximity and gene fusions in prostate cancer. *Science* 2009; **326**: 1230.

15 Dervan PB, Edelson BS. Recognition of the DNA minor groove by pyrrole–imidazole polyamides. *Curr Opin Struct Biol* 2003; **13**: 284–99.
16 Dervan PB. Molecular recognition of DNA by small molecules. *Bioorg Med Chem* 2001; **9**: 2215–35.
17 Trauger JW, Baird EE, Dervan PB. Recognition of DNA by designed ligands at subnanomolar concentrations. *Nature* 1996; **382**: 559–61.
18 Wang X, Nagase H, Watanabe T *et al.* Inhibition of MMP-9 transcription and suppression of tumor metastasis by pyrrole–imidazole polyamide. *Cancer Sci* 2010; **101**: 759–66.
19 Matsuda H, Fukuda N, Ueno T *et al.* Transcriptional inhibition of progressive renal disease by gene silencing pyrrole–imidazole polyamide targeting of the transforming growth factor-beta1 promoter. *Kidney Int* 2011; **79**: 46–56.
20 Nickols NG, Szablowski JO, Hargrove AE, Li BC, Raskatov JA, Dervan PB. Activity of a py-im polyamide targeted to the estrogen response element. *Mol Cancer Ther* 2013; **12**: 675–84.
21 Zhang Y, Sicot G, Cui X *et al.* Targeting a DNA binding motif of the EVI1 protein by a pyrrole–imidazole polyamide. *Biochemistry* 2011; **50**: 10431–41.
22 Ueno T, Fukuda N, Tsunemi A *et al.* A novel gene silencer, pyrrole-imidazole polyamide targeting human lectin-like oxidized low-density lipoprotein receptor-1 gene improves endothelial cell function. *J Hypertens* 2009; **27**: 508–16.
23 Takayama K, Kaneshiro K, Tsutsumi S *et al.* Identification of novel androgen response genes in prostate cancer cells by coupling chromatin immunoprecipitation and genomic microarray analysis. *Oncogene* 2007; **26**: 4453–63.
24 Hu Q, Kwon YS, Nunez E *et al.* Enhancing nuclear receptor-induced transcription requires nuclear motor and LSD1-dependent gene networking in interchromatin granules. *Proc Natl Acad Sci USA* 2008; **105**: 19199–204.
25 Obinata D, Takayama K, Urano T *et al.* Oct1 regulates cell growth of LNCaP cells and is a prognostic factor for prostate cancer. *Int J Cancer* 2012; **130**: 1021–8.
26 Obinata D, Takayama K, Urano T *et al.* ARFGAP3, an androgen target gene, promotes prostate cancer cell proliferation and migration. *Int J Cancer* 2012; **130**: 2240–8.
27 Lu S, Tsai SY, Tsai MJ. Regulation of androgen-dependent prostatic cancer cell growth: androgen regulation of CDK2, CDK4, and CKI p16 genes. *Cancer Res* 1997; **57**: 4511–6.
28 Li R, Wheeler T, Dai H, Frolov A, Thompson T, Ayala G. High level of androgen receptor is associated with aggressive clinicopathologic features and decreased biochemical recurrence-free survival in prostate: cancer patients treated with radical prostatectomy. *Am J Surg Pathol* 2004; **28**: 928–34.
29 Clark JP, Cooper CS. ETS gene fusions in prostate cancer. *Nat Rev Urol* 2009; **6**: 429–39.
30 Han B, Mehra R, Dhanasekaran SM *et al.* A fluorescence in situ hybridization screen for E26 transformation-specific aberrations: identification of DDX5-ETV4 fusion protein in prostate cancer. *Cancer Res* 2008; **68**: 7629–37.
31 Mehra R, Han B, Tomlins SA *et al.* Heterogeneity of TMPRSS2 gene rearrangements in multifocal prostate adenocarcinoma: molecular evidence for an independent group of diseases. *Cancer Res* 2007; **67**: 7991–5.
32 King JC, Xu J, Wongvipat J *et al.* Cooperativity of TMPRSS2-ERG with PI3-kinase pathway activation in prostate oncogenesis. *Nat Genet* 2009; **41**: 524–6.
33 Carver BS, Tran J, Gopalan A *et al.* Aberrant ERG expression cooperates with loss of PTEN to promote cancer progression in the prostate. *Nat Genet* 2009; **41**: 619–24.
34 Laxman B, Tomlins SA, Mehra R *et al.* Noninvasive detection of TMPRSS2:ERG fusion transcripts in the urine of men with prostate cancer. *Neoplasia* 2006; **8**: 885–8.
35 Leyten GH, Hessels D, Jannink SA *et al.* Prospective multicentre evaluation of PCA3 and TMPRSS2-ERG gene fusions as diagnostic and prognostic urinary biomarkers for prostate cancer. *Eur Urol* 2014; **65**: 534–42.
36 Cerveira N, Ribeiro FR, Peixoto A *et al.* TMPRSS2-ERG gene fusion causing ERG overexpression precedes chromosome copy number changes in prostate carcinomas and paired HGPIN lesions. *Neoplasia* 2006; **8**: 826–32.
37 Demichelis F, Fall K, Perner S *et al.* TMPRSS2:ERG gene fusion associated with lethal prostate cancer in a watchful waiting cohort. *Oncogene* 2007; **26**: 4596–9.
38 Shao L, Tekedereli I, Wang J *et al.* Highly specific targeting of the TMPRSS2/ERG fusion gene using liposomal nanovectors. *Clin Cancer Res* 2012; **18**: 6648–57.
39 Yang F, Nickols NG, Li BC, Marinov GK, Said JW, Dervan PB. Antitumor activity of a pyrrole–imidazole polyamide. *Proc Natl Acad Sci USA* 2013; **110**: 1863–8.
40 Raskatov JA, Nickols NG, Hargrove AE, Marinov GK, Wold B, Dervan PB. Gene expression changes in a tumor xenograft by a pyrrole-imidazole polyamide. *Proc Natl Acad Sci USA* 2012; **109**: 16041–5.
41 Raskatov JA, Hargrove AE, So AY, Dervan PB. Pharmacokinetics of Py-Im polyamides depend on architecture: cyclic versus linear. *J Am Chem Soc* 2012; **134**: 7995–9.
42 Nickols NG, Dervan PB. Suppression of androgen receptor-mediated gene expression by a sequence-specific DNA-binding polyamide. *Proc Natl Acad Sci USA* 2007; **104**: 10418–23.
43 Hagglof C, Hammarsten P, Stromvall K *et al.* TMPRSS2-ERG expression predicts prostate cancer survival and associates with stromal biomarkers. *PLoS ONE* 2014; **9**: e86824.
44 Selvaraj N, Budka JA, Ferris MW, Jerde TJ, Hollenhorst PC. Prostate cancer ETS rearrangements switch a cell migration gene expression program from RAS/ERK to PI3K/AKT regulation. *Mol Cancer* 2014; **13**: 61.
45 Tian TV, Tomavo N, Huot L *et al.* Identification of novel TMPRSS2:ERG mechanisms in prostate cancer metastasis: involvement of MMP9 and PLXNA2. *Oncogene* 2014; **33**: 2204–14.
46 Hanahan D, Weinberg RA. Hallmarks of cancer: the next generation. *Cell* 2011; **144**: 646–74.
47 Hagglof C, Bergh A. The stroma-a key regulator in prostate function and malignancy. *Cancers* 2012; **4**: 531–48.
48 Warrick JI, Tomlins SA, Carskadon SL *et al.* Evaluation of tissue PCA3 expression in prostate cancer by RNA in situ hybridization–a correlative study with urine PCA3 and TMPRSS2-ERG. *Mod Pathol* 2014; **27**: 609–20.
49 Huang KC, Dolph M, Donnelly B, Bismar TA. ERG expression is associated with increased risk of biochemical relapse following radical prostatectomy in early onset prostate cancer. *Clin Transl Oncol*, 2014; in press.
50 Berg KD, Vainer B, Thomsen FB *et al.* ERG protein expression in diagnostic specimens is associated with increased risk of progression during active surveillance for prostate cancer. *Eur Urol* 2014; in press.
51 Mani RS, Iyer MK, Cao Q *et al.* TMPRSS2-ERG-mediated feed-forward regulation of wild-type ERG in human prostate cancers. *Cancer Res* 2011; **71**: 5387–92.

Supporting Information

Additional supporting information may be found in the online version of this article:

Fig. S1. Distribution of FITC-labeled fusion and negative control polyamide in LNCaP cells. LNCaP cells were seeded on 24-well plates and cultured for 24 h, and then 5 μM of FITC-labeled fusion or negative control polyamide were applied to the growth medium. After 2 h incubation, medium was replaced with PBS containing Hoechst 33342, and cells were observed by fluorescence microscopy following 20 min incubation. Scale bar indicates 50 μm.

MOLECULAR CARCINOGENESIS 54:178–188 (2015)

Genome-Wide Screening of Aberrant DNA Methylation Which Associated With Gene Expression in Mouse Skin Cancers

Kyoko Fujiwara,[1,2]* Srimoyee Ghosh,[3] Ping Liang,[4] Evan Morien,[5] Masayoshi Soma,[1,2] and Hiroki Nagase[1,6]**

[1]*Innovative Therapy Research Group, Nihon University Research Institute of Medical Science, Nihon University School of Medicine, Tokyo, Japan*
[2]*Division of General Medicine, Department of Medicine, Nihon University School of Medicine, Tokyo, Japan*
[3]*Department of Zoology, North- Eastern Hill University, Shillong, Meghalaya, India*
[4]*Department of Biological Sciences, Brock University, St. Catharines, Ontario, Canada*
[5]*Department of Botany, University of British Columbia, Vancouver, British Columbia, Canada*
[6]*Division of Cancer Geneics, Chiba Cancer Center Research Institute, Chiba-shi, Chiba, Japan*

Epigenetic alteration of genomic DNA is a common and key process in carcinogenesis. There is considerable evidence indicating that some of the somatic alterations occurring during carcinogenesis in humans also involve the same processes as those observed in mice. Therefore, we analyzed mouse skin cancer tissues induced by the 2-stage carcinogenesis model to identify skin tumor-specific differentially methylated regions (ST-DMRs) during the multistep carcinogenesis process. We have previously identified ST-DMRs using the restriction landmark genomic scanning (RLGS) technique and reported that some of the mouse ST-DMRs were also epigenetically modified in human cancers, such as melanoma, neuroblastoma, and brain tumor. These results encouraged us to pursue global methylation screening in mouse skin carcinogenesis. Using the methylated DNA immunoprecipitation (MeDIP) method combined with the NimbleGen promoter plus CpG island (CpGi) array, we identified 615 ST-DMRs. In combination with global gene expression analysis, 91 of these ST-DMRs were shown to be located on or around the genes differentially expressed between normal skin and tumor tissues, including a candidate human tumor suppressor gene *Tfap2e*. As observed in human colorectal cancers, *Tfap2e* was methylated at a CpGi located in intron 3 and downregulated in skin tumors. Our results identified aberrant methylated regions that were associated with gene expression regulation during carcinogenesis, which may indicate critical genetic regions also involved in human carcinogenesis.

Key words: epigenetics; DNA methylation; squamous cell carcinoma; mouse model

INTRODUCTION

Epigenetic alteration of genomic DNA plays a crucial role in cancer initiation and development [1]. In particular, aberration of DNA methylation at the 5′-position of cytosine in the cancer genome has been extensively studied over the past few decades. It has been reported recently that DNA methyltransferases (DNMTs), which catalyze DNA methylation, are highly expressed or mutated in cancer tissues [2], and that member of the ten-eleven translocation (TET) proteins, which catalyze DNA demethylation, are mutated in in leukemia [3]. However the mechanisms controlling this dynamic change at 5-methylcytosine (5-mC) still remain elusive.

CpG dinucleotides in non-CpG islands (CpGis) are generally hypermethylated in normal cells but hypomethylated in some cancer cells. Global hypomethylation of DNA in colorectal cancer was one of the first reports of epigenetic abnormality [4]. Hypomethylation has been proposed to contribute to cancer development via generation of chromosomal instability, reactivation of transposable elements, and loss of imprinting [1]. DNA hypomethylation is also involved in the activation of oncogenes in cancer cells [5,6].

Abbreviations: CpGi, CpG island; ST-DMR, skin tumor-specific differentially methylated regions; DMBA, 7,12-dimethylbenz (a) anthracene; TPA, 12-O-tetradecanoylphorbol-13-acetate; MeDIP, methylated DNA immunoprecipitation; SCC, squamous cell carcinoma

Grant sponsor: National Institute of Environmental Health Services to H.N.; Grant number: ES012249; Grant sponsor: Roswell Park Alliance Foundation, in part, by the NCI Cancer Center; Grant sponsor: Roswell Park Cancer Institute; Grant number: CA016156; Grant sponsor: Academic Frontier Project for 2006 Project for Private Universities matching fund subsidy from MEXT to H.N; Grant sponsor: MEXT KAKENHI to H.N.; Grant number: 23300344; Grant sponsor: MEXT KAKENHI to K.F.; Grant number: 24591637

*Correspondence to: Innovative Therapy Research Group, Nihon University Research Institute of Medical Science, Nihon University School of Medicine, 30-1 Oyaguchi Kami-Cho, Itabashi, Tokyo 173-8610, Japan.

**Correspondence to: Chiba Cancer Center Research Institute, 666-2 Nitona-cho, Chuo-ku, Chiba-shi, Chiba 260, Japan.

Received 24 March 2013; Revised 8 August 2013; Accepted 14 August 2013

DOI 10.1002/mc.22085

Published online 24 September 2013 in Wiley Online Library (wileyonlinelibrary.com).

On the other hand, CpG sites in CpGis are usually unmethylated in normal cells but occasionally become aberrantly highly methylated in cancer cells [7]. Transcriptional inactivation of tumor suppressor genes by hypermethylation of their promoter CpGis is known to occur often in several cancer cells [8].

Because it is becoming clear that aberrant methylation is a promising molecular marker for early detection, prognosis, and prediction of drug response, global screening for aberrant methylation in the cancer genome has been actively performed [9–11]. Development of techniques for genome-wide DNA methylation analysis has enabled us to identify new aberrantly methylated regions in cancer genome DNA; however, these surveys may miss some candidate genes because of the technical pitfalls associated with genome-wide surveys. In prior studies, we have identified genomic regions showing differential methylation levels in mouse skin cancers induced by the 2-stage skin carcinogenesis model using the restriction landmark genomic scanning (RLGS) technique. We called these loci "skin tumor-specific differentially methylated regions (ST-DMRs)" and reported that these alterations were also found in human cancer tissues [12–14], including a new candidate gene *Zar1*, which showed very frequent aberrant methylation in various types of human cancers.

Importantly, the 2-stage skin carcinogenesis model is a multistage process and is similar to human tumor development in nature. A number of genetic alterations have been described in the mouse 2-stage skin carcinogenesis model involving RAS, cyclin D1 [15], RB1, TP53 [16], CDKN2A [17], pTen [18], and Aurka [19], which are also commonly found in human tumors. This underlying similarity in the biology of carcinogenesis in mice and humans implies that genes related to mouse tumor development may also be relevant to human tumor development. Importantly, animal model studies offer a number of distinct advantages over human studies, such as a genetically homogeneous population, well-controlled environment, and carcinogen or genetic manipulation.

Capitalizing on these advantages, we undertook a more comprehensive analysis of the aberrant methylation status of genomic DNA in mouse skin cancer tissues to find new genome loci. In addition, we performed global gene expression analysis of these tissues. The combination of both data sets will enable us to identify genes transcriptionally regulated by DNA methylation.

MATERIALS AND METHODS

Mice and Skin Cancer Induction

C57BL/6J (B6) female and male mice were purchased from Taconic (Germantown, NY) and maintained at the Department of Laboratory Animal Research at the Roswell Park Cancer Institute under an approved IACUC protocol. At 8 weeks of age, their backs were shaved with electric clippers 1 day before treatment initiation. 7,12-Dimethylbenz (a) anthracene (DMBA) and 12-O-tetradecanoylphorbol-13-acetate (TPA) were dissolved in acetone to obtain concentrations of 487.5 and 81 μM, respectively. Once a week, 200 μL of DMBA was injected into the back skin of the mice, and every week, 400 μL of TPA was applied 3 days after DMBA administration. After alternative treatment with DMBA and TPA for 5 weeks, the mice were treated with 400 μL of TPA twice a week for 20 weeks. The mice were assessed twice weekly for the appearance of papillomas during the promotion phase and monitored daily after the appearance of carcinomas. Skin papilloma and carcinoma samples were collected and frozen in liquid nitrogen and then stored at −80°C. The histology of each cancer and papilloma was assessed by a pathologist.

Global Analysis of Methylated DNA

Genomic DNA was extracted from fresh frozen tissues of two types of skin cancers obtained from two females and two males and from freshly frozen tissues of normal skin from one female and male (Table S1). Genomic DNA was extracted using the DNeasy Kit (Qiagen, Valencia, CA) according to the manufacturer's protocol.

Methylated DNA immunoprecipitation (MeDIP) analysis was performed for genome-wide methylation analysis of these DNAs, as described previously [20]. In brief, genomic DNA was digested with the restriction enzyme *Mse*I (New England Biolabs, Hertfordshire, UK) to produce 200- to 1000-bp fragments and then denatured by heating to produce single-stranded DNA. DNA fragments containing methylated CpG were immunoprecipitated with mouse monoclonal antibodies against 5-methyl cytidine (Eurogentec, Fremont, CA). After purification and validation, MeDIP and control DNA (the input DNA for MeDIP) were amplified using the Whole-Genome Amplification Kit (Sigma–Aldrich, St. Louis, MO) and then purified using a Quick PCR Purification Kit (Qiagen). Samples were sent to NimbleGen for analysis using a NimbleGen promoter plus CpGi array, which covers all UCSC-annotated 15 959 CpGi and 19 530 promoters for all RefSeq genes.

Methylation peaks were detected using NimbleScan software by searching for at least two neighboring probes showing significant methylation and listed in peak data files (.gff) (a detailed description is available at http://www.nimblegen.com). Using an in-house PERL script, each peak was categorized into one of the following: (a) promoter, located within an annotated promoter, which is 1-kb region flanking each side of the transcription start site (TSS); (b) intragenic, located in a gene excluding the promoter, as defined above; and (c) intergenic, located >2 kb away from

any annotated genes. All three groups were further categorized into two sub-groups, one being located at a site within 500 bp of CpGi and the other being located at a site >500 bp away from CpGi.

The processed data provided by NimbleGen were analyzed to identify the ST-DMRs. Using an in-house bioinformatics tool (available at http://genomics.brocku.ca/qinGE/index.html), two types of ST-DMRs were identified. The first was a set of methylation peaks commonly observed in all four samples of cancer tissues but not in normal skin, and the other was a set of methylation peaks commonly observed in both samples of normal skin but not in any of the cancer tissues.

To determine the significance of the ST-DMRs identified from our data sets over random chance, we performed Monte-Carlo simulation using simulated methylation peak data sets generated by randomizing the relationship between chromosome IDs and positions in the chromosome for all methylation peaks for each sample, followed by subjecting to the exact process of calling ST-DMRs as for the original methylation peaks. The numbers of the ST-DMRs from 1000 simulated data sets were used as the background noise for our DMR calling. To simulate the relationship between gene methylation and expression, 1000 sets of data sets with randomized relationship between the gene and its methylation category (hypermethylated or hypomethylated) and between gene and its expression category (upregulated, downregulated, or no change) were used to survey the occurrences of different relationships between methylation and gene expression by chance. Chi-square analysis was performed to compare the obtained DMR distributions and expected ones to evaluate the significance of the DMR distributions into different genomic regions.

MassARRAY Quantitative Methylation Analysis

A Sequenom MassARRAY Compact System was used for quantitative methylation analysis to confirm the results from MeDIP/NimbleGen. Genomic DNAs were extracted from four tissue samples for each of the normal skin, papilloma, and skin cancer tissues obtained from two females and two males (Table S1) using the DNeasy Kit (Qiagen) as described above. Then, 1 μg of the DNA samples was treated with sodium bisulfite using the EZ-96 DNA Methylation Gold Kit (Zymo Research, Irvine, CA). Primers were designed using MethPrimer [21] to span the methylation peaks and closely adjacent regions. Details of primer information along with PCR conditions are listed in Table 1. Bisulfite-treated DNA was amplified using HotStarTaq DNA polymerase (Qiagen) with specific primers. PCR products were treated with shrimp alkaline phosphatase and then subjected to in vitro transcription and RNase A cleavage for the T-reverse reaction, as described in the manufacturer's instructions. The samples were desalted and spotted on a 384-pad SpectroCHIP using a MassARRAY nanodispenser, followed by spectral acquisition on a MassARRAY Analyzer Compact MALDITOF MS. The resultant methylation calls were performed using EpiTYPER software v1.0 (Sequenom, San Diego, CA) to evaluate the quantitative methylation level of each CpG site or an aggregate of multiple CpG sites. The non-applicable reading and its corresponding site were eliminated during calculation.

RNA Isolation

RNA was extracted from skin tumor and normal skin tissues obtained from female and male mice. Some of the tissues are in common with the one used in the global genome methylation analysis also (Table S1). Skin and tumor tissues measuring 2–3 mm were homogenized using 1 mL of Trizol reagents (Life Technologies, Carlsbad, CA). Total RNA extracted from the homogenate was re-purified using the RNeasy Kit (Qiagen). The quality and quantity of total RNA were determined using an Agilent 2100 Bioanalyzer (Agilent Technologies, Palo Alto, CA). The quality-checked RNA samples were subjected to microarray and real-time PCR analyses.

Global Gene Expression Analysis

Total RNA samples extracted from two types of skin cancer obtained from two females and three males and two types of normal skins obtained from two females and three males were sent to Miltenyi Biotech (Bergisch Gladbach, Germany) for global gene

Table 1. Primer List

Target		Sequense
For expression analysis		
Tfap2e	Forward	ACCTATGCCGACAGCATGCCGA
Tfap2e	Reverse	TGTGTCAGACAGCTCTGCACC
For Sequenom Mass ARRAY EpiTyper		
Tfap2e exon1, 2	Forward	AGGAAGAGAGAGTGGAGTAGGTTGAGTTTAGAGG
Tfap2e exon1, 2	Reverse	CAGTAATACGACTCACTATAGGGAGAAGGCTCACCACTTCCTAAACTACCAAA
Tfap2e intron3	Forward	AGGAAGAGAGAGTGTTTTTTGGGAGAGTTT
Tfap2e intron3	Reverse	CAGTAATACGACTCACTATAGGGAGAAGGCTCTAAACCCCAAATCCTAAC

Tag-sequences for EpiTyper analysis are underlined.

expression analysis. In brief, 100 ng of each total RNA sample was reverse transcribed using the Low-Input RNA Linear Amplification Kit (Agilent Technologies) and then transcribed to Cy3-labeled cRNA according to the manufacturer's protocol. The qualified cRNA samples were hybridized to Agilent Whole Genome Oligo Microarrays 4×44K, and the fluorescence signals of all microarrays were detected by Agilent's Microarray Scanner System. The scanned data were processed using Agilent Feature Extraction Software (FES) to output the signal intensity of all probes in the arrays.

Normalization and further statistical analyses were performed using MultiExperiment Viewer v4.6 (http://www.tm4.org). Genes with a >2.0-fold difference in expression levels between normal skin and cancer tissues were further analyzed by statistical tests. An unpaired *t*-test was used to identify significantly different genes. *P*-values were computed from 10 000 permutations of the data for each gene.

Enrichment analysis of gene ontology was done for the differentially expressed genes using the BinGO [ref], which is a plugin software for Cytoscape (http://www.psb.ugent.be/cbd/papers/BiNGO/Home.html).

Quantitative Real-Time RT-PCR

Total RNA isolated from normal skin, papilloma, and cancer samples, obtained from two females and two males was used to synthesize cDNA by iScript (Bio-Rad, Hercules, CA). Real-time PCR was then performed using Takara Premix Ex Taq (Takara, Kyoto, Japan) to determine the gene expression level of Tfap2e.

Cell Culture and 5-Azacytidine Treatment

A mouse squamous cell carcinoma (SCC) cell line, which was established from SCC developed in FVB mice, was maintained in DMEM (Nakalai Tesque, Tokyo, Japan) containing 10% FBS (Nitirei Bioscience, Tokyo, Japan), 100 U/ml penicillin, and 0.1 mg/ml streptomycin (Gibco, Carlsbad, CA) in a humidified incubator at 37°C in 5% CO_2. The cells were treated with or without 5 μM 5-azacytidine (5-aza-dC, Sigma–Aldrich) for 72 h and then lysed in Trizol reagent. RNA and genomic DNA were purified from the Trizol lysate, and RNA was re-purified as described above.

RESULTS

Using the NimbleGen array analysis, two types of ST-DMRs were identified: (1) methylated only in cancer samples (hypermethylated DMR) and (2) methylated only in normal skin samples (hypomethylated DMR; Table 2). In this analysis, we identified a total of 5502 methylated regions that are common to all six samples, 77 ST-DMRs that are methylated in cancer tissues, but not in normal skins, and 538 ST-DMRs that specifically methylated in normal skins, but not in all four cancer tissues. This gives us a total of 615 ST-DMRs. All these three numbers were significantly higher than what could be expected from random chance, as simulated data sets generated from randomizing methylation peaks in position. The same set of the peak positions generate 13 ± 3.7, and 1.6 ± 0.9, and 170 ± 13.2 of common methylated region, hypermethylated ST-DMR and hypormethylated ST-DMRs, respectively ($P < 10^{-7}$ for the difference between observed value vs. random in all three cases). The significantly higher number of common methylated regions among all tissues, the two normal skins and the four cancer tissues over random chance is an indication of the biological similarity for the samples. The calculated false positives are ~2% and ~31.5% for hypermethylated, and hypomethylated ST-DMRs, respectively. The large discrepancy between

Table 2. Summary of ST-DMRs

Methylation status in cancer	Total	Promoter		Intragenic		Intergenic	
		CpGi	Non-CpGi	CpGi	Non-CpGi	CpGi	Non-CpGi
All ST-DMRs							
all probes	373,683	133 730 (35.8)	170 535 (45.6)	17 299 (5.7)	21 116 (2.6)	31 003 (8.2)	10 990 (2.9)
Hypermethylated	77	35 (45.5)	26 (33.8)	7 (9.1)	2 (2.6)	7 (9.1)	0 (0.0)
Hypomethylated	538	74 (13.8)	325 (60.4)	52 (9.7)	28 (5.2	41 (7.6	18 (3.3)

Methylation status in cancer	Expression level in cancer	Total	Promoter		Intragenic	
			CpGi	Non-CpGi	CpGi	Non-CpGi
ST-DMRs associated with the change of gene expression level						
Hypermethylated	Up-regulated	6	2 (33.3)	4 (66.7)	0 (0.0)	0 (0.0)
Hypermethylated	Down-regulated	4	1 (25.0)	1 (25.0)	2 (50.0)	0 (0.0)
Hypomethylated	Up-regulated	51	8 (15.7)	30 (58.8)	3 (5.9)	10 (19.6)
Hypomethylated	Down-regulated	30	5 (16.7)	20 (66.7)	4 (13.3)	1 (3.3)

Numbers in the parentheses indicate the percentage.

Table 3. List of ST-DMRs Associated With the Different Expression Level of Genes Between Skin Cancer and Normal Skin; Hypermethylated Loci Near Up-Regulated Genes

	Gene location		Nimblegen peak location		
Gene symbol	chr	Start–end	Start–end	CpGi	Position
(a)					
Artn	chr4	117424093–117427695	117427700–117427864	CpGi	TSS
Nol1	chr6	125097557–125110372	125110378–125110627	CpGi	TSS
4931440B09Rik	chr17	23564406–23571778	23571432–23571552	—	TSS
Oit3	chr10	58818316–58837136	58837058–58837148	—	TSS
Papola	chr12	106200700–106237910	106201064–106201166	—	TSS
Rabgap1l	chr1	162055850–162188248	162188248–162188815	—	TSS
(b)					
Npr2	chr4	43653034–43672344	43652538–43652838	CpGi	TSS
Slc45a3	chr1	133798154–133810510	133798058–133798178	—	TSS
Lhx2	chr2	38173316–38191737	38179036–38179156	CpGi	—
Tcfap2e	chr4	126218322–126238412	126234532–126235196	CpGi	—
(c)					
B3gnt3	chr8	74620707–74630781	74631112–74631197	CpGi	TSS
Creg2	chr1	39562951–39595728	39595405–39595539	CpGi	TSS
Dgcr2	chr16	17753917–17805232	17805171–17805251	CpGi	TSS
Dynll1	chr5	115559421–115561933	115561609–115561810	CpGi	TSS
Ephb2	chr4	135925683–136108011	136108922–136109356	CpGi	TSS
Ncl	chr1	88175889–88190626	88190100–88190349	CpGi	TSS
Rcc2	chr4	139973617–139993551	139974317–139974672	CpGi	TSS
Spnb4	chr7	27065142–27155349	27155073–27155422	CpGi	TSS
4933434I20Rik	chr8	86238576–86269507	86237275–86237839	—	TSS
Cd22	chr7	30574588–30589027	30588823–30588923	—	TSS
Cd5	chr19	10785187–10806019	10807576–10807677	—	TSS
Cd68	chr11	69480565–69482257	69481958–69482107	—	TSS
Cdc34	chr10	79085323–79091527	79091506–79091606	—	TSS
Cdc34	chr10	79085323–79091527	79092267–79092372	—	TSS
Cdh5	chr8	106990827–107033630	106989648–106990050	—	TSS
Col18a1	chr10	76495894–76610217	76611247–76611501	—	TSS
Cxcl1	chr5	91966509–91968315	91966668–91966983	—	TSS
Dnmt3l	chr10	77452970–77466744	77453123–77453238	—	TSS
Fscn1	chr5	143225510–143238323	143224216–143224860	—	TSS
Glp2r	chr11	67522624–67587348	67587468–67587758	—	TSS
Glp2r	chr11	67522624–67587348	67587906–67588122	—	TSS
Gpr84	chr15	103136268–103138472	103138422–103139046	—	TSS
Il24	chr1	132709619–132713542	132713654–132713798	—	TSS
Mag	chr7	30607942–30623592	30623314–30623453	—	TSS
Mid1	chrX	165029351–165344845	165323873–165323993	—	TSS
Olfr430	chr1	175906029–175906928	175906140–175906330	—	TSS
Olfr620	chr7	103485230–103486172	103485685–103485839	—	TSS
Osm	chr11	4136422–4141029	4136526–4136895	—	TSS
P2ry6	chr7	100811720–100838449	100838062–100838621	—	TSS
Pla1a	chr16	38315355–38352378	38352778–38352978	—	TSS
Rac2	chr15	78386423–78400038	78399747–78399891	—	TSS
Rassf1	chr9	107412756–107420361	107411472–107411627	—	TSS
Syt8	chr7	142244366–142249788	142242444–142242549	—	TSS
Tfpi2	chr6	3912594–3918356	3917857–3918006	—	TSS
Tlr6	chr5	65232240–65239169	65238988–65239131	—	TSS
Tnf	chr17	34807441–34810048	34810200–34810620	—	TSS
Trem1	chr17	47698177–47712333	47712507–47712787	—	TSS
Wnk1	chr6	119889956–120003398	119928811–119928955	—	TSS
Kcnb1	chr2	166794582–166880004	166796018–166796108	CpGi	—
Mid1	chrX	165029351–165344845	165341062–165341272	CpGi	—
Mid1	chrX	165029351–165344845	165342311–165342411	CpGi	—
Cd81	chr7	142862184–142877313	142871413–142871513	—	—
Kcnq1	chr7	142916643–143236432	142969543–142969614	—	—
Kcnq1	chr7	142916643–143236432	142991992–142992492	—	—
Kcnq1	chr7	142916643–143236432	142992846–142992946	—	—

Table 3. *(Continued)*

	Gene location		Nimblegen peak location		
Gene symbol	chr	Start–end	Start–end	CpGi	Position
Kcnq1	chr7	142916643–143236432	143074204–143074315	—	—
Kcnq1	chr7	142916643–143236432	143135848–143135943	—	—
Kcnq1	chr7	142916643–143236432	143182611–143182806	—	—
Kcnq1	chr7	142916643–143236432	143185491–143185591	—	—
Kcnq1	chr7	142916643–143236432	143191891–143191991	—	—
Myo7a	chr7	97926592–97992926	97982220–97982466	—	—
(d)					
Bach2	chr4	32567562–32909812	32567783–32567911	CpGi	TSS
Dnm3	chr1	163823978–164314705	164314872–164314996	CpGi	TSS
Gnal	chr18	67213704–67349624	67213275–67213377	CpGi	TSS
Paqr6	chr3	88450515–88454382	88451536–88451656	CpGi	TSS
Tnxb	chr17	34278590–34327683	34279992–34280390	CpGi	TSS
Adcy6	chr15	98418011–98435667	98435389–98435490	—	TSS
AU023871	chr17	34670748–34674240	34675827–34675927	—	TSS
Car6	chr4	149030814–149042270	149041974–149042133	—	TSS
Ccdc27	chr4	152870443–152886477	152885987–152886097	—	TSS
Cd247	chr1	167625397–167704109	167625400–167625710	—	TSS
Cd3e	chr9	44749737–44760585	44760255–44760535	—	TSS
Cdh13	chr8	121169721–122209431	121168695–121168849	—	TSS
Cyfip2	chr11	46037280–46155773	46079352–46079437	—	TSS
D16H22S680E	chr16	18214387–18238008	18237824–18237929	—	TSS
Gjb4	chr4	126853389–126856385	126856310–126856385	—	TSS
Gm128	chr3	95322510–95326610	95326035–95326285	—	TSS
Lamb2	chr9	108338048–108348632	108347850–108347965	—	TSS
Lpin1	chr12	16562115–16615250	16616254–16616524	—	TSS
Map3k13	chr16	21805951–21842030	21805868–21806312	—	TSS
Pon1	chr6	5118104–5143824	5144048–5144328	—	TSS
Pou6f1	chr15	100403351–100414399	100415073–100415158	—	TSS
Rccd1	chr7	80190146–80197937	80198705–80198795	—	TSS
Sytl2	chr7	90223890–90285630	90255161–90255610	—	TSS
Tcf7l2	chr19	55795517–55986492	55897965–55898294	—	TSS
Xlr3b	chrX	69507259–69518110	69519288–69519364	—	TSS
Bcl11b	chr12	108363029–108451028	108364698–108365062	CpGi	—
Dst	chr1	33956370–34252174	34122483–34122588	CpGi	—
Lgr6	chr1	136802763–136921687	136803973–136804407	CpGi	—
Scara5	chr14	64620536–64718936	64684872–64685126	CpGi	—
Cyfip2	chr11	46037280–46155773	46087736–46087916	—	—

CpGi, located on CpGi; TSS, transcription start site. Genome locations are shown according to NCBI36/mm8 assembly in UCSC genome browser.

the two categories of ST-DMRs is likely in part due to the larger number of methylation peaks and fewer number of samples for the normal skin group than for the cancer group.

In both types of ST-DMRs, >70% of the methylated loci were located in the promoter region. This proportion is not significantly different from that of the probe sets on NimbleGen array (Table 2). A total of 45.5% and 13.8% of the hypermethylated and hypomethylated ST-DMRs, respectively, were located in the CpGi promoter. These proportions are significantly higher for hypermethylated ST-DMRs and lower for hypomethylated ST-DMRs than the proportion expected by chance based on the distribution of probe sets in these regions on the NimbleGen array.

To identify ST-DMRs that may affect differential gene expression, global gene expression analysis of skin cancer tissues and normal skin was performed. The result was then compared with the data from global methylation analysis (Table 2). In this analysis, 2320 genes showed significantly higher expression and 1676 genes showed significantly lower expression compared with those in normal skin, with more than twofold change ($P < 0.01$). Among these genes, six gene showed higher expression and hypermethylation in SCC, four showed lower expression and hypermethylation, 51 showed higher expression and hypomethylation, and 30 showed lower expression and hypomethylation in SCC compared with those in normal skin samples. Among

hypomethylated ST-DMRs, the number of ST-DMRs associated with higher expression in cancer is significantly higher and that of ST-DMRs associated with lower expression is significantly lower than the expected values by chance ($P < 10^{-5}$, $P < 10^{-2}$, respectively). The detailed gene list is shown in Table 3a–d.

In the ontology analysis of those listed genes, it was shown that RNA processing related genes (*Papola, Nol1*) were enriched in the gene group exhibiting hypermethylation and higher expression in cancer (Table S2a). In the analysis of hypomethylated genes, genes involved in signal transmission (*Gpr84, Tnf, Olfr430, Wnk1, Tlr6, Ephb2, Olfr620, Osm, P2ry6, Spnb4, Rac2, Rassf1, Cd22,* and *Glp2r*) and regulation of cell proliferation (*Col18a1, Tnf, Rac2, Cd81, Cd5,* and *Cdh5*) were noticeable in the gene group with higher expression in the cancer samples than in the normal samples (Table S2b). Genes involved in immune response function (*Cd3e* and *Cd247*) and cell adhesion (*Cdh13, Tnxb, Lamb2, Cyfip2,* and *Dst*) were prominent in the gene groups with low expression in the cancer samples (Table S2c).

To confirm the data of global gene expression and methylation analysis, the expression of *Tfap2e*, which showed lower expression and higher methylation levels in the cancer samples than in the normal tissues, was analyzed by real-time PCR. As shown in Figure 1, the expression of *Tfap2e* was significantly lower in the cancer samples than in the normal skin samples, confirming the trend observed based on array-based expression analysis. The downregulation of this gene was also observed in the papilloma tissues. When the methylation level of the CpGi located in *Tfap2e* was assessed using the Sequenom MassARRAY, most of the CpG sites in the intron 3 CpGi showed hypermethylation in tumors and hypomethylation in normal skin (Figure 2B and D). The methylation level of the CpGi in the *Tfap2e* promoter region, which was not identified in the MeDIP/NimbleGen analysis, was also examined by MassARRAY; however, no clear difference was observed between the normal skin and tumors (Figure 2A and C).

To corroborate the effects of the methylation level of the intron 3 CpGi on the *Tfap2e* expression level, a SCC cell line was treated with or without 5-aza-dC, and the expression and DNA methylation levels of *Tfap2e* were analyzed. The cells incubated in the presence of 5-aza-dC showed a significantly higher expression of *Tfap2e* (Figure 3) and significantly lower methylation in the CpGi in the *Tfap2e* intron 3 (Figure 4B and D) compared with untreated cells. No clear difference was identified in the CpGi methylation in the *Tfap2e* promoter region between treated and untreated cells (Figure 4A and C).

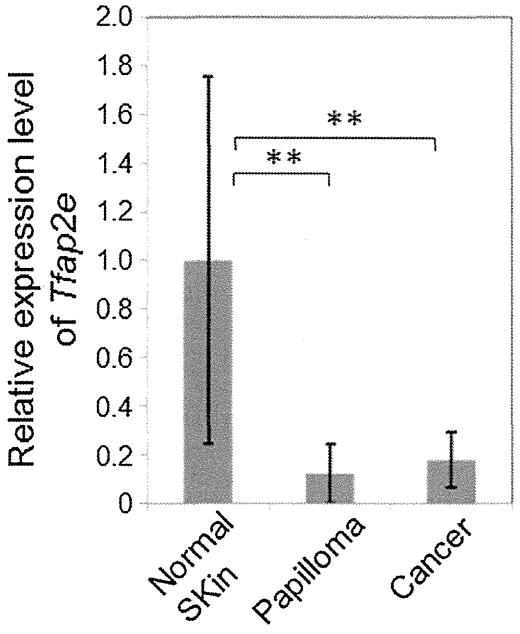

Figure 1. The expression level of *Tfap2e* in skin tumors and normal skin. Real-time PCR was performed to measure the expression level of *Tfap2e* in four samples each of normal skin, papilloma, and SCC. In each group, two were females and the other two were males. The experiment was performed twice, and the average ± SD of all experiment data are shown. Statistical significance was tested between papillomas or SCCs and normal skin, and shown as $^{**}P < 0.01$.

DISCUSSION

It was previously reported that the extent of loss of global genomic methylation is associated with the degree of tumor aggressiveness in mouse skin cancer cell lines. On the other hand, hypermethylated CpGi in tumor suppressor genes occurs in skin cancer cell lines and in the multistage mouse skin cancer model [22]. In that analysis, there were similar epigenetic changes in mouse and human SCC cell lines and primary skin tumor tissues. Using the RLGS technique, we also identified many loci that are epigenetically modified in mouse skin cancer tissues, and some of these loci have also been shown to be epigenetically modified in human cancer tissues [12–14]. To identify additional genomic loci that are aberrantly methylated in cancer tissues, we performed global screening for genome methylation using MeDIP in combination with NimbleGen array.

The present study identified 615 genetic loci that are aberrantly methylated in mouse skin cancer samples compared with normal skin samples. As is generally known based on the analysis of the cancer genome, majority of these ST-DMRs, that is, 538 of 615 loci, are hypomethylated in cancer tissues. Among all 615 ST-DMRs, >70% are located in promoter regions. This is almost same proportion of promoter CpGs/whole CpGs as represented in NimbleGen array. Interestingly, more than 45.5% of hypermethylated ST-DMRs are located in the CpGi promoter, and 33.8% are on non-CpGi promoter; on the other hand, only 13.8% of hypomethylated

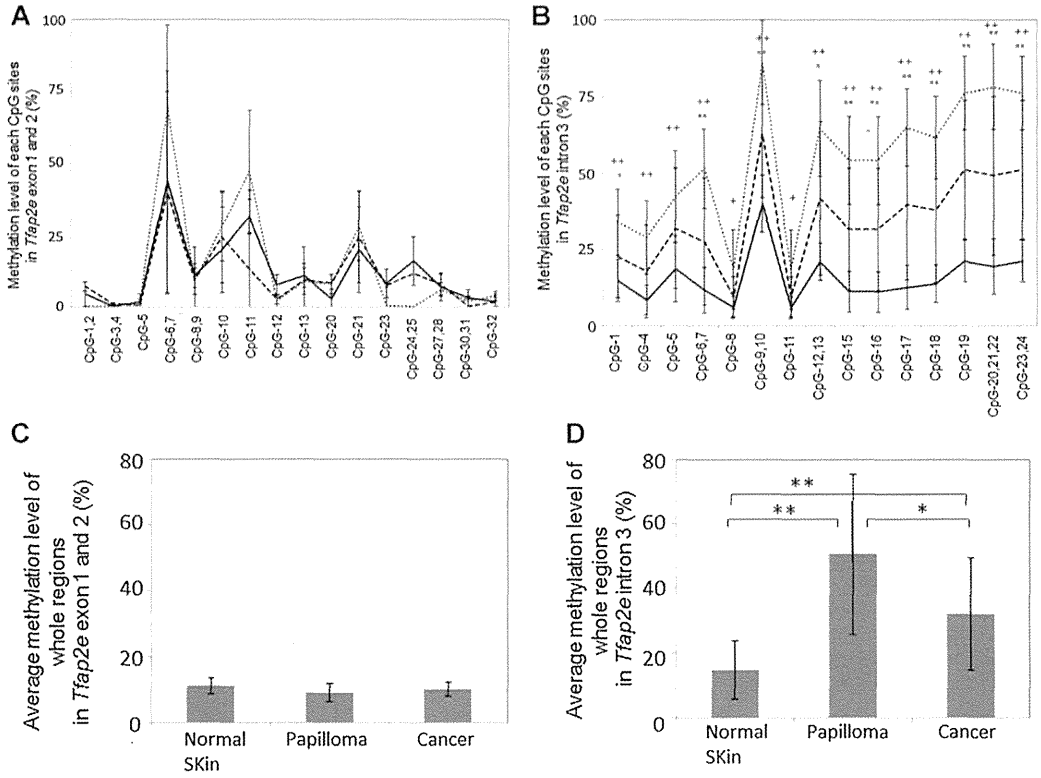

Figure 2. The methylation level of the *Tfap2e* genome CpGi in skin tumors and normal skin. The Sequenom MassARRAY EpiTyper was used to measure the methylation level of the *Tfap2e* genome CpGi in four samples each of normal skin, papilloma, and SCC. In each group, two were females and the other two were males. (A and C) Methylation level of the CpGi in *Tfap2e* exons 1 and 2. (B and D) Methylation level of CpGi in *Tfap2e* intron 3. The experiment was performed four times, and all the data were combined to calculate the average methylation level of each CpG site (A and B) and average methylation level of all the CpG sites within the CpGi (C and D). The solid line represents normal skin, dashed line SCC, and fine dashed line papilloma (A and B). Data are shown as the average ± SD. Statistical significance was tested between papillomas or SCCs and normal skin, shown as $^{*}P<0.05$, $^{**}P<0.01$ for SCC versus normal skin, and $^{+}P<0.05$, $^{++}P<0.01$ for papillma versus normal skin.

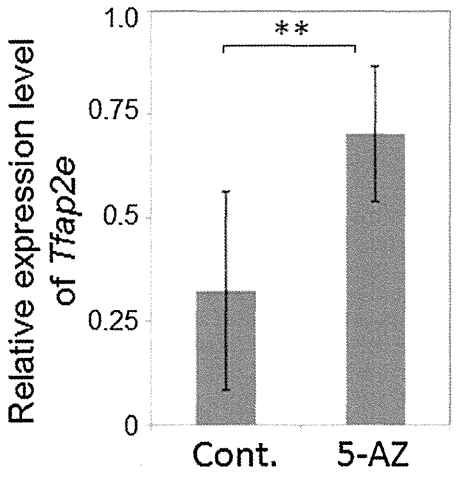

ST-DMRs are located on the CpGi promoter, and 60.4% are on non-CpGi promoter. When they are compared with the fixed set of regions represented on the NimbleGen arrays, those CpGi/non-CpGi proportions are significantly higher in hypermethylated ST-DMRs ($P<0.01$), and lower in hypomethylated ST-DMRs ($P<1\times10^{-6}$; Table 2). It has been reported that a number of genes with non-CpGi promoters are methylated in normal tissues. In the analysis of the genome methylation of mouse tissues, only approximately 10% of methylated CpGs are located on CpGi promoters, whereas almost 50% of methylated CpGs

Figure 3. Effect of 5-aza-dC treatment on the expression level of *Tfap2e* in the mouse SCC cell line. SCC cells were treated with or without 5 μM 5-aza-dC for 72 h, and the expression level of *Tfap2e* was measured using real-time PCR. Three samples were prepared for each condition, and the measurements were performed twice. All the data were combined to calculate average ± SD. Statistical significance is shown as $^{**}P<0.01$.

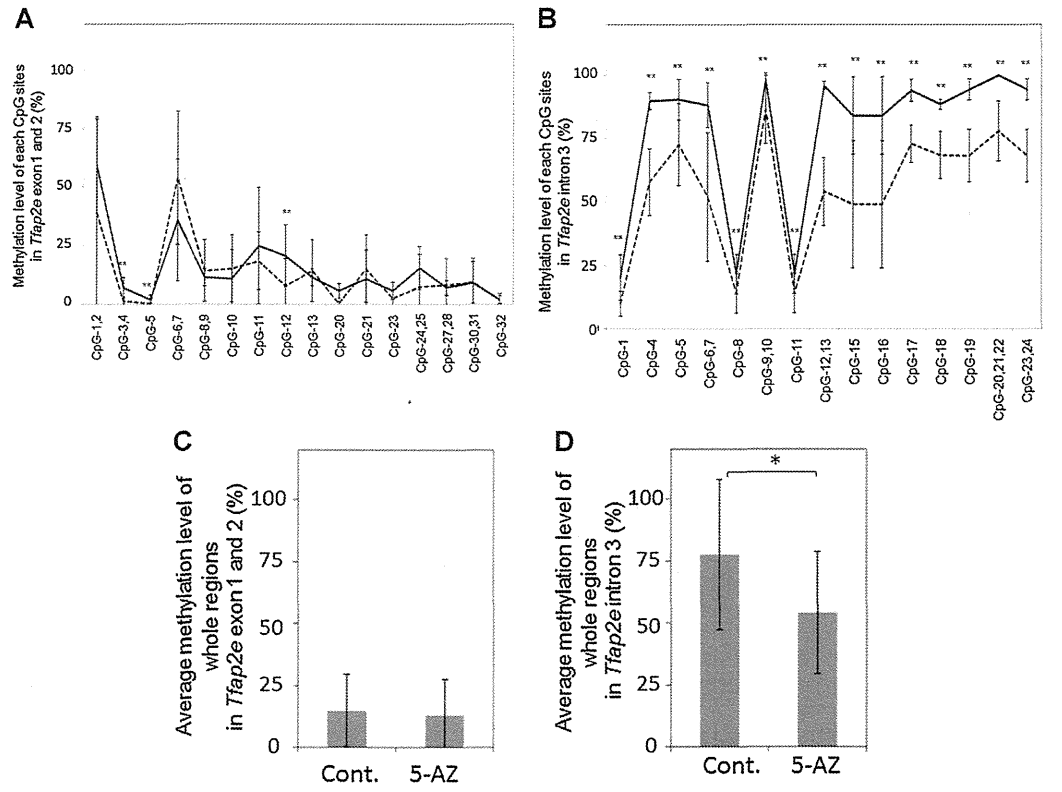

Figure 4. Effect of 5-aza-dC treatment on the methylation level of *Tfap2e* genome CpGi in the SCC cell line. SCC cells were treated with or without 5 μM 5-aza-dC for 72 h, and the methylation level of *Tfap2e* genome CpGi was measured using the Sequenom MassARRAY EpiTyper. A and C: Methylation level of the CpGi in *Tfap2e* exons 1 and 2. B and D: Methylation level of the CpGi in *Tfap2e* intron 3. The experiment was performed four times, and all the data were combined to calculate the average methylation level of each CpG site (A and B) and average methylation level of all CpG sites within the CpGi (C and D). The solid line represents control and dashed line 5-aza-dC treated cells (A and B). Data are shown as the average ± SD. Statistical significance is shown as $^{*}P < 0.05$ or $^{**}P < 0.01$.

are on non-CpGi promoters in normal tissues [20]. In the analysis of the methylation status of human chromosomes 6, 20, and 22, >87% of CpGi promoters were unmethylated and 2.1% were hypermethylated. On the other hand, only 20% of non-CpGi promoters were unmethylated, and 50% of these were hypermethylated in normal tissues [23]. The present analysis revealed distinct patterns in DNA methylation between normal and cancer tissues. Elevation of hypermethylation in CpGi promoter and loss of methylation in non-CpGi promoter seem to be the distinct features of cancer genome. The epigenetic signatures comprising DNA methylation, histone marks, and nucleosome occupancy of non-CpGi promoters are almost identical to CpGi promoters [24], suggesting that the aberrant methylation patterns of non-CpGi promoters may also contribute to tumorigenesis.

By combining our results with the data from global gene expression analysis, we also identified 91 ST-DMRs associated with an aberrant gene expression level in skin cancer tissues. *Tfap2e* was identified as one of the hypermethylated loci associated with reduced mRNA expression level. Using real-time PCR, we confirmed that the expression of *Tfap2e* was downregulated in both papilloma and SCC compared with normal skin. Using the MassARRAY Epityper method, we also confirmed that the methylation level of the CpGi in intron 3, but not that in the exon 1 or 2 region, was shown to be higher in the tumor tissues than in the normal tissues. The experiment using 5-aza-dC showed that the methylation level of the CpGi in the *Tfap2e* intron 3 was associated with the expression level of *Tfap2e*, but those of the CpGis in exons 1 and 2 were not. It was recently reported that CpGi within *TFAP2E* intron 3 was hypermethylated in 51% of human colorectal cancers, and the hypermethylation of *TFAP2E* was significantly associated with chemotherapy resistance. In humans, the methylation status of CpGi located in the *TFAP2E* intron 3 was associated with its expression level; however, CpGis on exons 1 and 2 did not show correlation with the expression level of this gene, as reported here in mice [25]. On the other hand,

hypermethylation of CpGi in *TFAP2E* exons 1 and 2 was reported to be a marker of human prostate cancer, although no information about the expression levels was presented [26].

*TFAP2*e is a member of the AP-2 transcription factor family. All of the five members have been known to play an important role in development [27]. *TFAP2*e is mainly expressed in neural tissue, particularly the adult midbrain and the midbrain and olfactory bulbs during mouse embryogenesis [28]. According to the CGAP database (http://cgap.nci.nih.gov/SAGE/AnatomicViewer), this gene is expressed in a relatively wide spectrum of organs, including the skin, in the adult mouse. Although the role of TFAP2E in tumor development is not well elucidated, the roles of other members of the AP-2 gene family, such as TFAP2A and TFAP2C, are well-known, that is, downregulation of TFAP2A and TFAP2C expression induced enhanced cell growth, invasion and resistance to anti-cancer drugs [29]. The AP-2 protein plays relevant roles in tumor development by regulating many types of key genes such as *P21waf1/Cip1* [30], *TGF-a* [31], *EGFR* [32,33], and *c-Myc* [34]. Our current data and these from previous reports suggest the possibility that *TFAP2*e also has a tumor suppressive effect; hence, its disruption by aberrant methylation could induce tumorigenic events in a conserved manner between mouse and humans.

In the list of aberrantly methylated and expressed genes in mouse skin cancer (Table 3a–d), some of those genes, such as *Lhx2*, *Wnk1*, *Cdh5*, *Cdh13*, *Rassf1*, and *Rac2* are also known to be aberrantly methylated in human cancer tissues. However, how these genes contribute to human tumorigenesis still remains elusive. Although differences in species can be attributed to their distinct genomic sequences and structures, a comparative approach enables us to find new aberrant genetic loci that may not otherwise be found during the analysis of human tissues, revealing the benefits of the experimental mouse model, including as the well-controlled genetic background, common etiology, and uniform breeding environment.

In summary, our study served as a proof of concept for identifying cancer-related genes using a combination of global screening for genomic DNA methylation and gene expression analyses of mouse skin cancers after treatment using the multistage skin carcinogenesis model. Using the MeDIP and NimbleGen array, combined with the Agilent microarray, we identified novel genes that are differentially methylated and expressed in skin tumors compared with normal skin. This study could provide evidence for a functional role of epigenetic regulation for skin cancer development after treatment of the skin cancer induced by the mouse 2-stage carcinogenesis model. Further functional studies of the genes listed in the tables may elucidate their role(s) in cancer development and progression.

ACKNOWLEDGMENTS

The authors thank Mr. M. Kataba, Ms. A.Oguni, Ms. T. Triplet and Ms. D. Tabaczynski for technical support and Ms. Kahoru Tagata for secretarial assistance. This research was supported by a grant from the National Institute of Environmental Health Services to H.N. (ES012249), the Roswell Park Alliance Foundation, in part, by the NCI Cancer Center Support Grant to Roswell Park Cancer Institute (CA016156), the Academic Frontier Project for 2006 Project for Private Universities matching fund subsidy from MEXT to H.N., MEXT KAKENHI Grant Number 23300344 to H.N., and MEXT KAKENHI Grant Number 24591637 to K.F.

REFERENCES

1. Esteller M. Epigenetics in cancer. N Engl J Med 2008;358: 1148–1159.
2. Shih AH, Abdel-Wahab O, Patel JP, Levine RL. The role of mutations in epigenetic regulators in myeloid malignancies. Nat Rev Cancer 2012;12:599–612.
3. Haffner MC, Chaux A, Meeker AK, et al. Global 5-hydroxymethylcytosine content is significantly reduced in tissue stem/progenitor cell compartments and in human cancers. Oncotarget 2011;2:627–637.
4. Feinberg AP, Vogelstein B. Hypomethylation distinguishes genes of some human cancers from their normal counterparts. Nature 1983;301:89–92.
5. Calvisi DF, Ladu S, Gorden A, et al. Mechanistic and prognostic significance of aberrant methylation in the molecular pathogenesis of human hepatocellular carcinoma. J Clin Invest 2007;117:2713–2722.
6. Shao C, Sun W, Tan M, et al. Integrated, genome-wide screening for hypomethylated oncogenes in salivary gland adenoid cystic carcinoma. Clin Cancer Res 2011;17:4320–4330.
7. Russo V, Martienssen R, Riggs A. *Epigenetic mechanisms of gene regulation. Plainview.* New York: Cold Spring Harbor Laboratory Press; 1996.
8. Jones PA, Baylin SB. The epigenomics of cancer. Cell 2007; 128:683–692.
9. Campan M, Moffitt M, Houshdaran S, et al. Genome-scale screen for DNA methylation-based detection markers for ovarian cancer. PLoS ONE 2011;6:e28141.
10. Fackler MJ, Umbricht CB, Williams D, et al. Genome-wide methylation analysis identifies genes specific to breast cancer hormone receptor status and risk of recurrence. Cancer Res 2011;71:6195–6207.
11. Poage GM, Houseman EA, Christensen BC, et al. Global hypomethylation identifies Loci targeted for hypermethylation in head and neck cancer. Clin Cancer Res 2011;17:3579–3589.
12. Shinojima Y, Terui T, Hara H, et al. Identification and analysis of *an early diagnostic marker for malignant melanoma:* ZAR1 intra-genic differential methylation. J Dermatol Sci 2010;59: 98–106.
13. Watanabe T, Yachi K, Ohta T, et al. Aberrant hypermethylation of non-promoter zygote arrest 1 (ZAR1) in human brain tumors. Neurol Med Chir (Tokyo) 2010;50:1062–1069.
14. Watanabe T, Yachi K, Ohta T, et al. Non-promoter hypermethylation of zygote arrest 1 (ZAR1) in human brain tumors. Brain Tumor Pathol 2011;28:199–202.
15. Wilkey JF, Buchberger G, Saucier K, et al. Cyclin D1 overexpression increases susceptibility to 4-nitroquinoline-1-oxide-induced dysplasia and neoplasia in murine squamous oral epithelium. Mol Carcinog 2009;48:853–861.